Robust Space Trajectory Design using Belief Optimal Control

Cristian Greco*
University of Strathclyde, Glasgow G1 1XJ, UK

Stefano Campagnola†
Jet Propulsion Laboratory, California Institute of Technology, Pasadena, CA 91109, USA

Massimiliano Vasile‡
University of Strathclyde, Glasgow G1 1XJ, UK

This paper presents a novel approach to the robust solution of optimal impulsive control problems under aleatory and epistemic uncertainty. The novel approach uses belief Markov decision processes to reformulate the control problem in terms of uncertainty distributions, called beliefs, rather than the realisations of the system states. This formulation leads to the definition of a Belief Optimal Control problem where the cost function and constraints are functions of the uncertainty distributions. The control formulation encompasses orbit determination arcs as well. The belief optimisation is solved with a shooting-like transcription and a nonlinear programming solver to optimise the resulting discretised problem. Both aleatory and epistemic uncertainties are propagated with a non-intrusive polynomial expansion to capture the nonlinearities of the dynamics. Finally, this new approach is applied to the robust optimisation of a flyby trajectory of the Europa Clipper mission in a scenario characterised by knowledge, execution and observation uncertainty.

I. Introduction and Motivation

SPACE trajectories are typically optimised to meet the science and flight system constraints in a nominal scenario. However, in real-life applications, perfect compliance to the reference trajectory is impossible to achieve as uncertainty always affects the system; uncertainty can be due to imperfect state knowledge, imperfectly known dynamical parameters, missed thrust events and execution errors.

In the design phase, the robustness and reliability of the reference trajectory are usually evaluated a posteriori through a navigation analysis and the nominal design adjusted through several iterations. The robustness and reliability evaluation is carried out by assessing the mission outcome when the trajectory is affected by different uncertainty

*PhD Candidate, Aerospace Centre of Excellence, University of Strathclyde, *c.greco@strath.ac.uk* (Corresponding author).
†Mission Design Engineer, Outer Planet Mission Analysis Group, *stefano.campagnola@jpl.nasa.gov*; Member AIAA.
‡Professor, Aerospace Centre of Excellence, University of Strathclyde, *massimiliano.vasile@strath.ac.uk*; Member AIAA.

realisations. In order to improve robustness, common practice is to either add a posteriori empirical margins [1, 2], and enforced coasting arcs for trajectory correction manoeuvres, reduce the thrust level or increasing the flyby altitudes. Hence, the optimisation of the nominal trajectory is generally decoupled from the quantification of the uncertainty in its realisation. The iteration and handover between trajectory design and navigation analysis are generally time-consuming and may lead to sub-optimal trajectories with over-conservative margins.

Recent developments in components and launchers are now enabling deep-space microsat and nanosat missions. Such spacecraft have limited orbit control capabilities (e.g., limited ΔV and thrust levels), large uncertainties in the state knowledge (limited ground station access) and in the execution (low Technology Readiness Level components), and limited room for margins and system redundancy (limited size and cost) [3, 4]. For these reasons, microsats are more prone to early failure [5]. Therefore, for these missions, there is a compelling reason to design for robustness and reliability from the start. Furthermore, one can argue that, while trajectory optimisation under uncertainty is an enabling methodology for small spacecraft, it presents advantages also for larger scale traditional missions. In fact, integrating uncertainty from the start of the design process leads to optimal trajectories that achieve a better compromise between performance and robustness than deterministic ones with added empirical margins. It also reduces the number of iterations between trajectory design and navigation analysis with a corresponding saving in cost, time and complexity.

In the past few decades, a number of authors have addressed the problem of introducing either aleatory or epistemic uncertainty, or both, in the design of space trajectories.

One alternative is to formulate trajectory design under aleatory uncertainty as a stochastic optimal control problem. Such formulation was then tackled with model predictive control [6] and stochastic closed-loop control [7] to account for correction terms in the control profile. Stochastic differential dynamic programming was applied to trajectory optimisation with an expected value formulation for Gaussian-modelled uncertainties [8]. Tube stochastic optimal control generalised this approach to tackle nonlinear constrained problems under uncertainty by approximating generic stochastic processes as Gaussian and employing chance-constraints on the open and closed-loop control [9]. Covariance control [10, 11] was specialised and applied for spacecraft guidance [12] and control design [13] around asteroids. Risk-aware trajectory optimisation was proposed by using chance-constrained stochastic optimal control under Gaussian uncertainties with a convex optimisation approach for impulsive controls [14] or with primer vector theory for continuous thrust [15].

Other works focused on the impact of specific uncertainty sources on the trajectory of a spacecraft. The case of a temporary engine failure was investigated by stochastic programming [16, 17]. A method based on Taylor polynomials algebra was developed to deal with uncertain boundary conditions around a reference trajectory and produce a robust guidance law [18]. The use of expected thrust fraction was investigated to design continuous thrust trajectories which are resilient to missed thrust events [19, 20]. Also, the use of machine learning techniques is being studied for spacecraft guidance and control [21] under uncertainty, e.g. using neural networks [22, 23] or reinforcement learning [24, 25].

Approaches based on evidence theory to model epistemic uncertainty were developed for the robust optimisation of transfers under system and dynamical uncertainties [26–28]. A generalisation to multi-objective problems and uncertainty modelled with p-boxes was developed to compute families of control laws and tested on a rendezvous scenario [29].

However, these methods do not include a rigorous navigation analysis in the optimisation loop to quantify flight dynamics and science requirements. In particular, the Orbit Determination (OD) process with measurements simulations and uncertainty update is not included in previous works. In addition, some of the previous approaches deal with uncertainties of a single nature while employing a tailored formulation to address a specific application.

In this context, this paper presents a novel development in optimal control under observation and model uncertainty for the robust design of space trajectories. The paper introduces an optimal control formulation that allows the integrated treatment of a mix of aleatory (irreducible probabilistic variability) and epistemic (lack of knowledge) uncertainty. The idea is to insert both types of uncertainty, generally affecting manoeuvre execution and navigation analysis, in the formulation of optimal control problems via a Belief Markov Decision Process (BMDP) model [30]. The result is a belief formulation of optimal control problems, or Belief Optimal Control (BOC). In BOC, the goal is to control the time evolution of the belief state induced by partially or non observable uncertain variables rather than controlling the realisations of a stochastic variable (or process) with known distribution. In practical terms, this means controlling a distribution function, or a family of distributions, induced by the uncertain variables, over a set of partially observable states coming from an inference process. The solution of the BOC is an open-loop control profile which is the most robust and reliable against the effects of uncertainty.

This work builds on and extends previous research on optimal control under epistemic uncertainty [31, 32]. In [32] the authors introduced a new multiple shooting transcription approach for trajectory optimisation under uncertainty. The new transcription approach was capable of handling a wide range of uncertainty models (parametric, non-parametric, imprecise set of distributions, etc.), while keeping the familiar notation of deterministic optimal control problems. This paper extends the multiple shooting transcription method to incorporate a navigation analysis in the robust trajectory optimisation problem under aleatory and epistemic uncertainty. This approach enables the direct coupling of trajectory optimisation and navigation analysis by incorporating the quantification of navigation uncertainty within the optimisation cycle. To this end, this paper also introduces an efficient Uncertainty Quantification (UQ) approach for nonlinear Navigation Analysis (NA), based on non-intrusive polynomial representations, which generalises existing linear NA methods [33–35]. The trajectory is segmented into arcs and on each arc a set of states, coming from uncertainty in observation realisations and manoeuvre execution errors, are propagated with a non-intrusive polynomial expansion. When observations are available, state and associated uncertainty predictions are updated with Bayes inference. Thus, the full distribution over all possible states is retained during the dynamical propagation and the computation of the objective and constraints, in contrast to most methods in literature which rely on expected value and covariance only.

We will test the BOC method on the robust optimisation of a leg of the Europa Clipper flyby tour [36], a scenario where proper uncertainty treatment is crucial to ensure appropriate close-approach conditions and low probability of impact. BOC is employed to optimise the total ΔV while satisfying a set of constraints on the *expected value* of the terminal states. The uncertainty considered in this paper stems from knowledge error in the initial spacecraft state, from execution errors introduced by the thrust pointing and magnitude inaccuracies when operating the engine, and by measurement and sensor noise.

The remainder of the paper is structured as follows. Section II introduces the Belief Optimal Control formulation and is followed by Section III where a transcription method is developed to convert the BOC into a Nonlinear Programming (NLP) problem. Specifically, this section addresses how to incorporate measurements in the trajectory design process, presents the polynomial NA, and discusses practical strategies to propagate and quantify uncertainty in different cases. In Section IV, the BOC is applied to the robust optimisation of one leg of the Europa Clipper flyby tour. The outcome is a trajectory that is simultaneously statistically optimal and reliable. Finally, Section V concludes the paper with some final remarks and a discussion on potential future applications.

II. Belief Optimal Control Formulation

A generic deterministic Optimal Control Problem (dOCP) with impulsive controls can be formulated as

$$\min_{\mathbf{u}} \; J = \Phi(t_F, \mathbf{x}_f) + \int_{t_0}^{t_F} L(t, \mathbf{x}, \mathbf{u})\, dt \tag{1a}$$

$$\text{s.t.} \quad \dot{\mathbf{x}} = f(t, \mathbf{x}, \mathbf{d}, \mathbf{u}) \tag{1b}$$

$$\mathbf{g}(t, \mathbf{x}, \mathbf{d}, \mathbf{u}) \in \boldsymbol{G} \tag{1c}$$

$$\boldsymbol{\psi}(t_0, \mathbf{x}_0, t_F, \mathbf{x}_f) \in \boldsymbol{\Psi}\ , \tag{1d}$$

where t is the independent variable, $\mathbf{x} \in \mathbb{R}^{n_x}$ is the state vector, $\mathbf{d} \in \mathbb{R}^{n_d}$ are static model parameters, $\mathbf{g} \in \mathbb{R}^{n_g}$ are path constraints, and $\boldsymbol{\psi} \in \mathbb{R}^{n_x}$ is a set of boundary conditions. Controls $\mathbf{u}(t)$ are in the form:

$$\mathbf{u}(t) = \sum_i \mathbf{u}_i \delta(t - t_i) \tag{2}$$

with δ the Dirac delta function and $\mathbf{u}_i \in \mathbb{R}^{n_u}$.

When boundary conditions and system parameters are affected by uncertainty, problem (1) needs to be recast in a form that allows one to derive a control law that is optimal with respect to a metric that accounts for the effect of uncertainty. In the remainder of this section, we propose a belief formulation of optimal control problems that allows one to directly work with the probability distributions of the uncertain quantities and to incorporate system-level and

navigation uncertainties in the derivation of optimal control laws.

A. Preliminary Definitions

In this section, we define a number of elements that are required to introduce the belief formulation of optimal control problems.

- *Uncertainty model.* In this paper, we employ a mixed aleatory and epistemic uncertainty model where a generic uncertain variable $\mathbf{Z} : \Omega_{\mathbf{Z}} \to \mathbb{R}^{n_z}$, with samples space $\Omega_{\mathbf{Z}}$, has an associated probability density function (pdf) $p(\mathbf{z}; \boldsymbol{\lambda})$ parameterised with the epistemic parameter $\boldsymbol{\lambda} \in \Omega_{\boldsymbol{\lambda}}$. Thus, this model assumes that the aleatory uncertainty, characterised by the pdf p, is imprecise due to epistemic uncertainty affecting the parameters $\boldsymbol{\lambda}$. The epistemic set of parametric distributions is defined as

$$\mathcal{P}_{z,\lambda} = \left\{ p(\mathbf{z}; \boldsymbol{\lambda}) \,|\, \boldsymbol{\lambda} \in \Omega_{\boldsymbol{\lambda}} \right\} , \tag{3}$$

  where $\Omega_{\boldsymbol{\lambda}}$ is the epistemic parameter domain. When information is sufficient to identify a single distribution, uncertainty is purely aleatory and $\Omega_{\boldsymbol{\lambda}}$ is a singleton. For ease of notation, in the following, we will use uppercase special characters $Z_{\boldsymbol{\lambda}} = p(\mathbf{z}; \boldsymbol{\lambda})$ to indicate the pdf of a random variable $\mathbf{Z}$. The explicit dependence on the epistemic parameter $\boldsymbol{\lambda}$ will be dropped when not essential.

  We will consider such uncertainty model in the initial conditions and static system and model parameters. They are assumed to be random variables $\mathbf{X}_0 : \Omega_{\mathbf{X}_0} \to \mathbb{R}^{n_x}$ and $\mathbf{D} : \Omega_{\mathbf{D}} \to \mathbb{R}^{n_d}$, with sample spaces respectively $\Omega_{\mathbf{X}_0}$ and $\Omega_{\mathbf{D}}$ and pdfs $p(\mathbf{x}_0; \boldsymbol{\lambda}_{x_0})$ and $p(\mathbf{d}; \boldsymbol{\lambda}_d)$. We will write:

$$\mathbf{X}_0 \sim p(\mathbf{x}_0; \boldsymbol{\lambda}_{x_0}) \in \mathcal{P}_{x_0;\boldsymbol{\lambda}_{x_0}} \tag{4}$$

$$\mathbf{D} \sim p(\mathbf{d}; \boldsymbol{\lambda}_d) \ \in \mathcal{P}_{d;\boldsymbol{\lambda}_d} \ . \tag{5}$$

  to indicate that the uncertain variables $\mathbf{X}_0$ and $\mathbf{D}$ are described by a mixed aleatory and epistemic model parametrised in $\boldsymbol{\lambda}_{x_0}$ and $\boldsymbol{\lambda}_d$ respectively. In the remainder of the paper we will present the methodology starting from the treatment of epistemic uncertainty, under the assumption of a known family of distributions, and then derive the solution for aleatory uncertainty as a special case for $\boldsymbol{\lambda}$ precisely known.

- *Probability metric.* Given a quantity of interest $f \in \mathscr{F}$ and the set $\mathcal{P}_{z,\lambda}$ in Eq. (3) we define a functional

$$F_\lambda : \mathcal{P}_{z,\lambda} \times \mathscr{F} \to \mathbb{R} \tag{6}$$

  from the function and probability sets to the real line. A common integral form of such functional is the expectation

of a function f with respect to the distribution $p(\mathbf{z};\boldsymbol{\lambda})$

$$\mathbb{E}_{\boldsymbol{\lambda}}\big[f\big] = \int_{\Omega_{\mathbf{z}}} f(\mathbf{z})\, p(\mathbf{z};\boldsymbol{\lambda})\, d\mathbf{z}\,. \tag{7}$$

The inferior and superior values of F_λ over the set $\mathcal{P}_{z,\lambda}$ are named lower bound $\underline{F}$ and upper bound $\overline{F}$ respectively. For the epistemic specification as in Eq. (3) the lower and upper bounds are defined as

$$\underline{F} = \inf_{\boldsymbol{\lambda}\in\Omega_{\boldsymbol{\lambda}}} F_\lambda\big(\mathbf{z};\boldsymbol{\lambda}\big) \tag{8a}$$

$$\overline{F} = \sup_{\boldsymbol{\lambda}\in\Omega_{\boldsymbol{\lambda}}} F_\lambda\big(\mathbf{z};\boldsymbol{\lambda}\big)\,. \tag{8b}$$

For the special case of aleatory uncertainty, we have $\underline{F} = \overline{F}$ because Ω_λ is a singleton. Consider, for example, the probability P that the quantity of interest ϕ is below a given threshold ϕ^*, then we can write:

$$F_\lambda = P(\phi(\mathbf{z}) < \phi^*) = \int_{\Omega_z} \mathbb{1}_{(\phi(\mathbf{z})<\phi^*)}(\mathbf{z})\, p(\mathbf{z};\boldsymbol{\lambda})\, d\mathbf{z} \tag{9}$$

where $\mathbb{1}$ is the indicator function.

- *Execution errors*. The general form of the *executed* control $\mathbf{U}_e(\mathbf{u},\mathbf{X}) : \mathbb{R}^{n_u}\times\mathbb{R}^{n_x}\to\mathbb{R}^{n_u}$ considered in this paper is a random variable defined as

$$\mathbf{U}_e(\mathbf{u},\mathbf{X}) = \sum_i [\overline{\mathbf{u}}_i + \delta\mathbf{u}_i(\mathbf{X}) + \boldsymbol{\Theta}_i(\mathbf{u}_i + \delta\mathbf{u}_i)]\delta(t-t_i)\,, \tag{10}$$

where $\overline{\mathbf{u}}_i$ and $\delta\mathbf{u}_i$ are the *commanded* open- and closed-loop control terms respectively, and $\boldsymbol{\Theta}_i$ models the control errors. When present, the execution errors are included in the uncertain model parameters $\mathbf{D}$. The sum of the commanded components is denoted as $\mathbf{u}_i = \overline{\mathbf{u}}_i + \delta\mathbf{u}_i$. In this form, we assume that the control uncertainty is affecting only the components of the manoeuvre and not the time of the execution, and is a function of the commanded control. The meaning and form of the feedback component and errors will be better defined in the remainder of the paper.

- *Observation uncertainty*. Observations are employed to reduce the knowledge uncertainty associated to the system state. The observation model is a nonlinear function of the state and environment noise realisations $\boldsymbol{\varepsilon}_k$:

$$\mathbf{y}_k = h(\mathbf{x}_k, \boldsymbol{\varepsilon}_k)\,. \tag{11}$$

Hence, a generic observation $\mathbf{y}_k \in \mathbb{R}^{n_y}$ is a realisation of the random variable $\mathbf{Y}_k : \Omega_{\mathcal{E}_k} \to \mathbb{R}^{n_y}$ induced by the

sensor noise $\mathcal{E}_k$. The random variable observation is described by the conditional likelihood

$$\mathbf{Y}_k \sim p(\mathbf{y}_k | \mathbf{x}_k; \boldsymbol{\lambda}_y) \in \mathcal{P}_{y;\boldsymbol{\lambda}_y} \ . \tag{12}$$

This relation expresses that, given the state, the observation likelihood $\mathcal{Y}_k = p(\mathbf{y}_k | \mathbf{x}_k; \boldsymbol{\lambda}_y)$ is completely determined by the sensor noise $\mathcal{E}_k$ [37]. At each observation k, the state distribution is updated given the last received observation according to an inference rule $\mathcal{T}_I$ which returns the posterior distribution, conditional on all the observations received until time t_k, as

$$\mathcal{X}_k = \mathcal{T}_I\left(\mathcal{X}_k^-, \mathcal{Y}_k\right) = p(\mathbf{x}_k | \mathbf{y}_{1:k}) \ , \tag{13}$$

given the predicted state uncertainty $\mathcal{X}_k^- = p(\mathbf{x}_k | \mathbf{y}_{1:k-1})$ and the last observation $\mathbf{y}_k$. The superscript $(\cdot)^-$ indicates the predicted distribution right before the new observation $\mathbf{y}_k$ is received.

- *Dynamical evolution*. $\mathbf{X}_0$ and $\mathbf{D}$, together with the dynamical equation (1b), induce the state at a later time to be a random variable $\mathbf{X}$ through the push-forward measure resulting from the pointwise dynamical flow. The distribution of the random variable $\mathbf{X}$ evolves according to a Partial Differential Equation (PDE), written in the general notation

$$\partial_t \mathcal{X} - \mathcal{F}_x(t, \mathcal{X}, \mathcal{D}, \mathcal{U}_e) = 0 \ , \tag{14}$$

where the term $\mathcal{F}_x$ includes the partial derivatives with respect to the state variables, and it depends on the pointwise dynamics (1b). Eq.(14) is the Fokker-Planck (or Forward Kolmogorov) equation [38]. Epistemic uncertainty on either of the sources of uncertainty induces, through the dynamical evolution, the state distribution at a later time to be set-valued itself as

$$\mathbf{X} \sim X = p(\mathbf{x}; \boldsymbol{\lambda}) \in \mathcal{P}_{\mathbf{X};\boldsymbol{\lambda}} \ , \tag{15}$$

where $\boldsymbol{\lambda} = [\boldsymbol{\lambda}_{x_0}, \boldsymbol{\lambda}_d, \boldsymbol{\lambda}_y]$ is the collection of all the epistemic parameters.

B. Belief Formulation

Given the elements defined in the previous section, the optimal control problem under uncertainty is well described as a Partially Observable Markov Decision Process [39], i.e. the state is observed only through indirect measurements. This model can be re-framed as a BMDP [30], which employs an advantageous belief state representation. That is, the state of the model is not a specific realisation $\mathbf{x}$, but rather the state is the density function $\mathcal{X}$. The probability distribution of the dynamical system state is henceforth called *belief* state. An advantage of such formulation is that the belief state

can be computed at any time even if the specific state realisation is not observable. We write the BOC as

$$\min_{\bar{\mathbf{u}}} \sup_{\boldsymbol{\lambda}} \left\{ C_F\left(t_F, \mathcal{X}_f\right) + \int_{t_0}^{t_F} C\left(t, \mathcal{X}, \mathcal{U}_e\right) dt \right\} \tag{16a}$$

$$\text{s.t.} \begin{cases} \partial_t \mathcal{X} - \mathcal{F}_x(t, \mathcal{X}, \mathcal{D}, \mathcal{U}_e) = 0 & \text{between observation times} \\ \mathcal{X}_k = \mathcal{T}_I\left(\mathcal{X}_k^-, \mathcal{Y}_k\right) & \text{at each observation } k \end{cases} \tag{16b}$$

$$\underline{G}\left(t, \mathcal{X}, \mathcal{D}, \mathcal{U}_e\right) \in \boldsymbol{\Phi}_{\underline{\mathbf{G}}}\,, \qquad \overline{G}\left(t, \mathcal{X}, \mathcal{D}, \mathcal{U}_e\right) \in \boldsymbol{\Phi}_{\overline{\mathbf{G}}} \tag{16c}$$

$$\underline{\Psi}\left(t_0, \mathcal{X}_0, t_F, \mathcal{X}_f\right) \in \boldsymbol{\Phi}_{\underline{\boldsymbol{\Psi}}}\,, \quad \overline{\Psi}\left(t_0, \mathcal{X}_0, t_F, \mathcal{X}_f\right) \in \boldsymbol{\Phi}_{\overline{\boldsymbol{\Psi}}} \tag{16d}$$

$$\mathcal{X}_0 \in \mathcal{P}_{\mathbf{X}_0;\boldsymbol{\lambda}_{x_0}},\ \mathcal{D} \in \mathcal{P}_{\mathbf{D};\boldsymbol{\lambda}_d},\ \mathcal{Y}_k \in \mathcal{P}_{\mathbf{Y}_k;\boldsymbol{\lambda}_y} \tag{16e}$$

where, C_F and C are the functionals (7) associated respectively to Φ and L, $\underline{G}$, $\overline{G}$, $\underline{\Psi}$, $\overline{\Psi}$, are the lower and upper limits defined in (8a) and (8b) on the functionals (7) associated to the path and boundary constraints $\mathbf{g}$ and $\boldsymbol{\psi}$. The target sets $\boldsymbol{\Phi}_{\underline{\mathbf{G}}}$, $\boldsymbol{\Phi}_{\overline{\mathbf{G}}}$, $\boldsymbol{\Phi}_{\underline{\boldsymbol{\Psi}}}$ and $\boldsymbol{\Phi}_{\overline{\boldsymbol{\Psi}}}$ for the expectations on $\mathbf{g}$ and $\boldsymbol{\psi}$ are predefined quantities. The objective in (16a) is the upper bound of the objective function realisations under uncertainty. Eqs. (16b) describe how the belief state evolves in time according to a PDE and is updated with an inference rule each time an observation of the state is acquired. They are the dual of the equations of motion (1b) in the dOCP. Finally, Eq.(16e) describes the uncertainty structure of the problem, namely expressing the initial condition for the belief state, the uncertain parameter distribution and the observation likelihood. As previously stated, the execution errors are included in the uncertain model parameters $\mathbf{D}$.

The BOC aims at optimising the open-loop component to find the nominal trajectory which minimises the objective function and satisfies the constraints under uncertainty. In general, the BOC problem (16) has no closed-form solution, just like the deterministic dOCP (1). Thus, in the following section, we propose a direct transcription method that allows incorporating navigation analysis in the optimisation of the control law under the type of epistemic and observation uncertainty defined in this section.

III. Transcription Method

Solving problem (16) requires the propagation of the belief state from the initial conditions through the dynamics, and to update it with observations. This section presents an efficient multiple shooting-like direct transcription method for the solution of problem (16), which employs a direct propagation of the belief state. This work generalises the direct transcription method developed in [32] to the case in which orbit determination arcs intermingle control arcs and a fully intrusive uncertainty propagation is not possible.

A. Sequential Belief Transcription

Following the same idea of general multiple shooting schemes, we start by partitioning the independent variable domain into segments. In this case, we partition the time domain into the following time segments:

$$[t_k, t_{k+1}] \quad \text{for } k = 0, 1, \ldots, F-1 \,. \tag{17}$$

On each segment we define a vector of commanded control parameters $\mathbf{u}_k$ in the following form:

$$\mathbf{u}_k(t_k, \mathbf{X}_k) = \overline{\mathbf{u}}_k(t_k) + \delta\mathbf{u}_k\big(\mathbf{X}_k\big) \tag{18}$$

where the first term is an unknown parameter to be optimised, whereas the second one is a correction to $\overline{\mathbf{u}}_k(t_k)$ coming from a pre-defined function of the state at time t_k. Operationally speaking, the term $\overline{\mathbf{u}}_k(t_k)$ has to be understood as an open-loop control while $\delta\mathbf{u}_k\big(\mathbf{X}_k\big)$ as a feedback control policy. From (10) the executed controls $\mathbf{U}_{e_k}$ at time t_k is:

$$\mathbf{U}_{e_k} = \mathbf{u}_k(t_k, \mathbf{X}_k) + \boldsymbol{\Theta}_k(\mathbf{u}_k(t_k, \mathbf{X}_k), \boldsymbol{\lambda}_k) \,, \tag{19}$$

which combines the commanded controls with execution errors.

In addition, on each segment we define a vector of uncertain parameters $\mathbf{D}_k$ such that:

$$\mathbf{D} = \big[\mathbf{D}_0, \ldots, \mathbf{D}_k, \ldots, \mathbf{D}_{F-1}\big] \,. \tag{20}$$

This decoupling holds under the condition that $\mathbf{D}_k$ affects the dynamics only over the time interval $t \in [t_k, t_{k+1}]$. For instance, the errors due to manoeuvres executed in a given temporal interval influence the belief state until the end time of that interval. Observation errors are another example of uncertainty sources that affect the belief state update at a given time only. The effect of these errors, beyond the end of the interval where they manifest, is carried by the belief state at the start of the next interval. Uncertainties that affect the dynamics over multiple time segments are replicated across all the segments they affect, e.g. dynamical model parameters. This decoupling enables one to favourably exploit the Markov property of the system that stems from the BMDP formulation.

For each time segment, the belief state $\mathcal{X}_k$ is first propagated from t_k to t_{k+1} under the effect of the dynamics (1b) and the possible control actions $\mathbf{u}_k$, if they are present on that segment. We indicate this propagation with the symbol $\mathcal{T}_P$ that represents the mapping of the probability distribution $p(\mathbf{x}_k \,|\, \mathbf{y}_{1:k})$ from t_k to t_{k+1}:

$$\mathcal{X}_{k+1}^{-} = \mathcal{T}_P\big(\mathcal{X}_k, \mathcal{D}_k, \mathcal{U}_{e_k}\big) = p(\mathbf{x}_{k+1} \,|\, \mathbf{y}_{1:k}) \,. \tag{21}$$

We now consider the case of observation instances at the end of some sub-intervals $[t_k, t_{k+1}]$. Thus, suppose now that a new measurement $\mathbf{y}_{k+1}$ is available. By using Bayes' inference rule one can calculate the posterior distribution:

$$\mathcal{X}_{k+1} = \mathcal{T}_I\left(\mathcal{X}_{k+1}^-, \mathcal{Y}_{k+1}\right) = p(\mathbf{x}_{k+1} \mid \mathbf{y}_{1:k+1}) = \frac{p(\mathbf{y}_{k+1}|\mathbf{x}_{k+1})\, p(\mathbf{x}_{k+1} \mid \mathbf{y}_{1:k})}{\int p(\mathbf{y}_{k+1}|\mathbf{x}_{k+1})\, p(\mathbf{x}_{k+1} \mid \mathbf{y}_{1:k})\, d\mathbf{x}_{k+1}} \ . \tag{22}$$

Again, the dependencies on the deterministic parameters have not been written explicitly. We assume that the measurement $\mathbf{y}_{k+1}$ is conditionally independent of the observation and control history, given the state at time t_{k+1}, thus those terms disappear from the observation likelihood $p(\mathbf{y}_{k+1}|\mathbf{x}_{k+1})$.

Hence, the calculation of the belief state at time t_{k+1} can be written, in compact form, as the composition of the state propagation map $\mathcal{T}_P$ and the Bayes inference map $\mathcal{T}_I$:

$$\mathcal{X}_{k+1} = \mathcal{T}\left(\mathcal{X}_k, \mathcal{D}_k, \mathcal{U}_{e_k}, \mathcal{Y}_{k+1}\right) = \mathcal{T}_I \circ \mathcal{T}_P \ . \tag{23}$$

Eq. (23) models the most general case of a segment where both control actions at t_k and measurements at t_{k+1} are present. In the following, arcs can have both control and observations, only control actions, only observations or neither of the two (pure propagation). Depending on the specific case, we will apply either the propagation map alone, the inference map or the composition of the two.

One interesting feature of the belief formulation is that, while the system pointwise state would dynamically evolve through a one-to-many relationship in a standard Markov Decision Process, the belief state of the Belief Markov Decision Process evolves through the prediction and update steps according to a one-to-one relationship.

Being the uncertain parameters partitioned as $\mathbf{D} = \left[\mathbf{D}_0, \ldots, \mathbf{D}_k, \ldots, \mathbf{D}_{F-1}\right]$, the main advantage of the shooting scheme is that it decouples the uncertainty in the different time segments $[t_k, t_{k+1}]$. When the belief is propagated from t_k to t_{k+1}, the stochastic dimensionality is $n_{\xi_k} = n_x + n_{d_k}$, where n_x and n_{d_k} are respectively the state and uncertain parameters $\mathbf{D}_k$ dimensionality, instead of being the total $n_\xi = n_x + n_d$ as it would be with a vanilla Monte Carlo approach. This efficient decoupling avoids the accumulation of uncertainty and the growth of the belief stochastic dimension in time, thus helping to contain the curse of dimensionality, typical of uncertainty quantification problems. This feature is computationally crucial for an uncertainty quantification method which is called within an optimisation loop numerous times.

B. The Propagation Map $\mathcal{T}_P$

Propagating the belief state in time is the most computationally intensive step of the transcription method as it would require solving a PDE which has no closed-form solution in the general nonlinear case. For this reason, some approximations are typically introduced to speed up the uncertainty propagation. Among them, the most widely used are

linearised dynamics around the reference trajectory, linearised observation model and Gaussian-assumed uncertainty distributions [34, 35, 40].

When these approximations are enforced, the mean and covariance of each belief component are propagated in time with inexpensive matrix multiplications. Furthermore, as the observation model is linearised, the uncertainty update at observation times in Eq. (22) reduces to the simple analytical linear Kalman Filter update. The main limitation comes from the need to linearise the dynamics. A further limitation is the number of statistical moments that are propagated since the general approach is to retain only mean and covariance.

The BOC formulation, however, permits the propagation of the exact dynamics and, in the general case, of a family of probability distributions. Thus we propose to split the mapping $\mathcal{T}_P$ in two steps: first we create a polynomial representation of all possible states at time t_{k+1} given the states at time t_k, the uncertain parameters and the control variables; then we sample the distribution at time t_k to represent the distribution at time t_{k+1}. This second step requires only multiple evaluations of the polynomial at time t_{k+1}. This technique was introduced in [41] using an intrusive polynomial algebra [42]. Here we propose a non-intrusive approach more tailored for black-box dynamical models instead.

Consider the set $\Omega_{\boldsymbol{\xi}_k}$ of all possible uncertainty realisations $\boldsymbol{\xi}_k = [\mathbf{x}_k, \mathbf{d}_k, \mathbf{u}_{e_k}]^T$ at time t_k, recalling that the executed control realisation $\mathbf{u}_{e_k}$ is derived from the definition of the executed control in Equation (19). In the epistemic setting, the samples $\boldsymbol{\xi}_k$ are drawn from a family of distributions dependent on the epistemic parameters $\boldsymbol{\lambda}$. Thus, the sampling set $\Omega_{\boldsymbol{\xi}_k}$ needs to be chosen large enough to allow drawing a sufficient number of samples to build a good approximation of $\mathcal{T}_P$, for all values of the epistemic parameters. The set $\mathcal{F}_k^{k+1}$ of compatible states at time t_{k+1} can be defined as

$$\mathcal{F}_k^{k+1} = \{\mathbf{x}_{k+1}(\boldsymbol{\xi}_k) \,|\, \boldsymbol{\xi}_k \in \Omega_{\boldsymbol{\xi}_k}\} \,, \tag{24}$$

where $\mathbf{x}_{k+1}(\boldsymbol{\xi}_k)$ is defined as

$$\mathbf{x}_{k+1}(\boldsymbol{\xi}_k) = \mathbf{x}_k + \int_{t_k}^{t_{k+1}} f(t, \mathbf{x}, \mathbf{d}_k, \mathbf{u}_{e_k}) \; dt \,. \tag{25}$$

The goal is now to construct a polynomial function that maps the set $\Omega_{\boldsymbol{\xi}_k}$ to the set $\mathcal{F}_k^{k+1}$ in the form:

$$\mathbf{x}_{k+1} = F_k^{k+1}(\boldsymbol{\xi}_k) = \sum_{i=0}^{\infty} \alpha_{k,i} \, \Psi_i(\boldsymbol{\xi}_k) \quad \forall \boldsymbol{\xi}_k \in \Omega_{\boldsymbol{\xi}_k} \,, \tag{26}$$

where Ψ_i is the *i-th* multivariate polynomial basis and $\alpha_{k,i}$ its coefficient. For practical applications, this expansion is truncated to a finite order q and only the first N_q terms are retained:

$$F_k^{k+1}(\boldsymbol{\xi}_k) \approx \widetilde{F}_k^{k+1}(\boldsymbol{\xi}_k) = \sum_{i=0}^{N_q} \alpha_{k,i} \, \Psi_i(\boldsymbol{\xi}_k) \,. \tag{27}$$

In this paper the coefficients $\alpha_{k,i}$ are computed using stochastic collocation [43]: a number of samples $\mathbf{x}_{k+1}$ is first evaluated over a structured grid of collocation points $\boldsymbol{\xi}_k^{(j)}$; then a polynomial approximation $\widetilde{F}_k^{k+1}$ is built to fit the set of $\mathbf{x}_{k+1}$ vectors. Because the stochastic and control dimensions can be rather large, the Smolyak polynomial space variant [44] is used to limit the growth of collocation points with increasing stochastic dimensions. The third-party open-source library Sparse Grids Matlab Kit is employed to construct the polynomial representation [45]. Figure 1 shows an example of a grid coming from a full tensor product (a) and a sparse Smolyak grid (b) both constructed with a level two grid, that is 17 nodes per dimension.

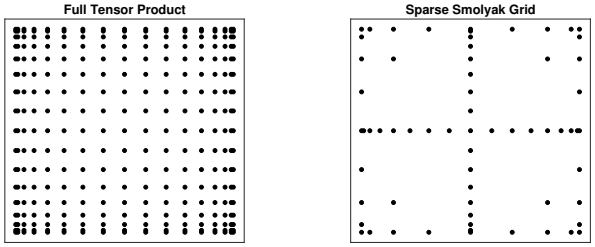

(a) (b)

Fig. 1 Comparison of two-dimensional grids constructed by (a) full tensor product and (b) sparse Smolyak rule of one-dimensional grids.

The grid level is a tunable parameter that determines the number of collocation points in each dimension. Samples are unique across different grid levels. Therefore, one can sequentially increment the grid level while reusing previously computed samples until reaching the requested accuracy. To assess the surrogate accuracy, one option is to construct a polynomial representation by using a collocation grid of level $\bar{l}$. Then, the accuracy can be quantified as the root mean square error of the polynomial mapping versus the numerical one on a subset of samples of grid level $\bar{l}+1$. If such error is below a user-set threshold, the polynomial representation is accepted, otherwise, the polynomial is re-constructed with a collocation grid of level $\bar{l}+1$ and the process iterated until the requested accuracy is met.

There are several advantages of this sparse polynomial mapping by stochastic collocation over other methods for uncertainty propagation in trajectory optimisation applications:

- being a non-intrusive method, the dynamical model is called as a black-box function, thus pre-existing libraries can be easily interfaced with such transcription without alteration;
- the accuracy of the approximation in Equation (27) can be made as good as desired by increasing the degree q of the polynomial space; the growth of the number of collocation points with the degree q is limited by the sparse Smolyak variant;
- Chebyshev polynomials are employed for their global convergence properties over a compact set [42] and previous applications in a number of aerospace cases [32, 46, 47].

Once the polynomial $\widetilde{F}_k^{k+1}$ is available, the propagation map $\mathcal{T}_P$ can be approximated as

$$\mathcal{T}_P \approx p\big(\widetilde{F}_k^{k+1}(\boldsymbol{\xi}_k) \,|\, \mathbf{y}_{1:k}\big) \,. \tag{28}$$

C. Navigation Analysis and the Inference Map $\mathcal{T}_I$

The inference map $\mathcal{T}_I$ comes from the simulation of the expected observations along the trajectory considering observation errors. Furthermore, for a given observation at time t_k the measurement $\mathbf{y}_k$ is conditional to the actual state $\mathbf{x}_k$ of the spacecraft which is uncertain. Thus one needs to simulate a set of possible measurements over the space of possible predicted states [48, 49].

Considering M measurement realisations $\mathbf{y}_k^{(j)}$, with $j = 1, \ldots, M$, each with an associated probability density, an inference step is required for each of them. This results in a set of possible posterior beliefs

$$\mathcal{X}_k^{(j)} = p\left(\mathbf{x}_k \,|\, \mathbf{y}_{1:k}^{(j)}\right) \,, \tag{29}$$

each resulting from a different observation realisation. Each of these posterior beliefs is then propagated to t_{k+1}. Such scenario is depicted in Figure 2, where multiple belief states are generated as a consequence of the inference with multiple sample measurements. Specifically, Figure 2(a) depicts the uncertainty propagation in time without any observation. The belief state at time t_k and the the propagated one at time t_{k+1} are represented with dark and light blue ellipses, respectively. Figure 2(b) indicates the generation of multiple observation samples by Monte Carlo at t_k, represented in yellow. Figure 2(c) shows the multiple uncertainty updates of the belief given the Monte Carlo observation samples as green ellipses. Figure 2(d) depicts the updated belief components propagation after the new observations have been processed. Hence, we first apply the inference map (22) M times, one for each $\mathbf{y}_k^{(j)}$ at time t_k,

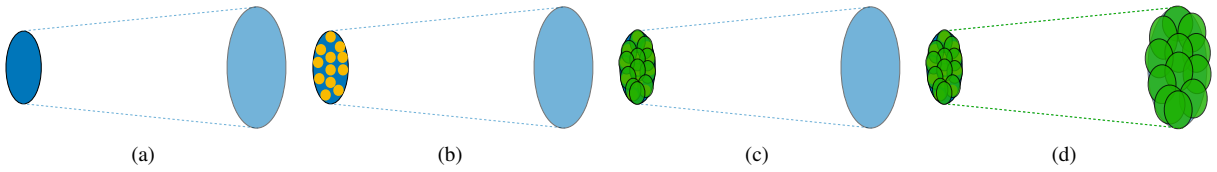

Fig. 2 Different steps of Monte Carlo measurement simulation on the uncertainty propagation process: (a) propagation without observations; (b) observations simulation; (c) beliefs update; (d) updated beliefs propagation.

then we use map (28) to propagate each posterior to obtain M distributions at time t_{k+1}.

If this process was iterated for each time segment, one would have an exponential growth of the number of expected trajectories and associated control laws. Indeed, if we were to simulate M new observations for each belief component at time t_{k+1}, we would end up with M^2 belief components, which would grow to M^3 at t_{k+2}, and so on. On the contrary,

we build the following convex combination once the M distributions at time t_{k+1} are available:

$$\begin{aligned} \mathcal{X}_{k+1}^{-} &= \sum_{j=1}^{M} b^{(j)}\, \mathcal{X}_{k+1}^{-(j)} \\ \sum_{j=1}^{M} b^{(j)} &= 1 \,, \end{aligned} \tag{30}$$

where $b^{(j)}$ is the *belief degree*, a weight quantifying the relative degree of likeliness of each $\mathcal{X}_{k+1}^{(j)}$. The value of each $b^{(j)}$ depends on the credibility of each measurement $\mathbf{y}_k^{(j)}$. Then, we use this belief state as prior at time t_{k+1} to be updated with the M simulated likelihoods. With this approach, the number of belief components is kept constant to M regardless of the number of shooting segments.

The convex combination in Eq. (30) can be derived from the concept of Jeffrey conditionalisation [50]. This conditionalisation rule describes how the probability of the occurrence of an event A depends on the realisation of events $B^{(j)}$ with confidence belief degrees $b^{(j)}$:

$$\Pr\left(A \mid B^{(1)} \equiv b^{(1)}, \ldots, B^{(M)} \equiv b^{(M)}\right) = \sum_{j=1}^{M} b^{(j)} \Pr\left(A \mid B^{(j)}\right) , \tag{31}$$

when the condition events form a partition. This conditionalisation generalises the traditional conditional probability measure, which is now a special case when event $B^{(j)}$ has been observed with certainty, i.e. when its belief degree is $b^{(j)} = 1$, and therefore the belief degree of its conjugate is zero. Given this probability measure, we can interpret the belief in Eq. (30) as an overall inference step by Jeffrey conditionalisation over sampled observations $\mathbf{y}_k^{(j)}$ with belief degrees $b^{(j)}$:

$$\mathcal{X}_k \;=\; p\big(\mathbf{x}_k \mid \mathbf{y}_k^{(1)} \equiv b^{(1)}, \ldots, \mathbf{y}_k^{(M)} \equiv b^{(M)}\big) = \sum_{j=1}^{M} b^{(j)}\, p\big(\mathbf{x}_k | \mathbf{y}_k^{(j)}\big) \tag{32}$$

The problem is that, in general, the sampled observations do not form a partition of the observation space which is indeed continuous. However, we can approximate any continuous distribution as a probability mass function by using samples drawn from the original one and the Dirac delta function as [51]

$$p(\boldsymbol{\xi}) \approx \sum_{j=1}^{M} b^{(j)} \delta\big(\boldsymbol{\xi} - \boldsymbol{\xi}^{(j)}\big) \,. \tag{33}$$

If such approximation is introduced for the observation likelihood, then the Jeffrey conditionalisation provides a key formal interpretation of the employed inference step with different sampled measurements for the navigation analysis approach considered.

D. Solution of the Transcribed Problem

Once the belief state is propagated at each stage k with the approximated propagation map $\mathcal{T}_P$ and the inference map $\mathcal{T}_I$ is applied when observations are available, Problem (16) is transcribed into the following NLP problem:

$$
\begin{aligned}
&\min_{\bar{\mathbf{u}}} \sup_{\boldsymbol{\lambda}} \left\{ C_F\left(t_F, \mathcal{X}_f\right) + \sum_k \sum_s w_s C\left(t_s, \mathcal{X}_k, \mathcal{U}_{e_k}\right) \right\} \\
&\text{s.t.} \begin{cases} \mathcal{X}_{k+1}^- = \mathcal{T}_P\left(\mathcal{X}_k,\, \mathcal{D}_k,\, \mathcal{U}_{e_k}\right) & \text{between observation times} \\ \mathcal{X}_k = \mathcal{T}_I\left(\mathcal{X}_k^-, \mathcal{Y}_k\right) & \text{at observation instances} \end{cases} \\
&\quad \underline{G}_k\left(t_k, \mathcal{X}_k, \mathcal{D}_k, \mathcal{U}_{e_k}\right) \in \mathbf{\Phi}_{\underline{\mathbf{G}}_k}\,, \quad \overline{G}_k\left(t_k, \mathcal{X}_k, \mathcal{D}_k, \mathcal{U}_{e_k}\right) \in \mathbf{\Phi}_{\overline{\mathbf{G}}_k} \\
&\quad \underline{\Psi}\left(t_0, \mathcal{X}_0, t_F, \mathcal{X}_f\right) \in \mathbf{\Phi}_{\underline{\mathbf{\Psi}}}\,, \qquad \overline{\Psi}\left(t_0, \mathcal{X}_0, t_F, \mathcal{X}_f\right) \in \mathbf{\Phi}_{\overline{\mathbf{\Psi}}} \\
&\quad \mathcal{X}_0 \in \mathcal{P}_{\mathcal{X}_0},\ \ \mathcal{D} \in \mathcal{P}_{\mathcal{D}},\ \ \mathcal{Y}_k \in \mathcal{P}_{\mathcal{Y}_k;\boldsymbol{\lambda}_y}
\end{aligned}
\tag{34}
$$

where w_s are quadrature weights used to discretise the objective integral in time. The outer optimisation is carried out on the transcribed open-loop control components to find the most robust and reliable nominal trajectory. The quantities C_F,C, G_k, Ψ are integrals over the space of the uncertain parameters as in Eq. (7). In the general case, these integrals need to be computed numerically, either by sampling or with a numerical quadrature formula, as

$$
\mathbb{E}[\phi(\mathbf{Z}); \boldsymbol{\lambda}] = \int \phi(\mathbf{z})\, p(\mathbf{z}; \boldsymbol{\lambda})\, d\mathbf{z} \approx \sum_k w_i(\boldsymbol{\lambda})\, \phi(\mathbf{z}_i)\,, \tag{35}
$$

where ϕ can be Φ, L, $\mathbf{g}$ or $\boldsymbol{\psi}$.

For given control vector and epistemic parameter to evaluate, the transcription complexity depends primarily on the number of aleatory variables and observation arcs. The number of grid samples to construct the expansion by sparse collocation scales polynomially with the number of aleatory dimensions, whereas the complexity of evaluating the surrogate for samples' propagation is secondary. Updating the belief state requires only simple evaluations of the likelihood function and low-dimensional matrix operations, as discussed in the next sections. Hence, the main computational and accuracy advantages of the transcription come from the shooting discretisation. This transcription enables an efficient decoupling of the uncertainties and, therefore, lower aleatory dimensions in each segment. Thus, adding new control or observation instances does not yield an exponential increase in computational complexity.

The two-level NLP problem is solved by nested local optimisations. Under epistemic uncertainty, for each integral (35) we need to solve an optimisation problem over the space of the parameters $\boldsymbol{\lambda}$. To alleviate the computational burden of these optimisations, the polynomial mapping in (27) is constructed only once per iteration of the minimisation over the space of the controls, and the optimisations over $\boldsymbol{\lambda}$ are performed exploiting the inexpensive surrogate model. This is made possible by the fact that the mapping (27) covers the entire space of uncertainties by construction. This approach

causes the input set $\Omega_{\boldsymbol{\xi}_k}$ to be larger than in the purely aleatory case. Nonetheless, the collocation grid level can be tuned to ensure the required surrogate accuracy under epistemic uncertainty as well. Thus, propagation of uncertainty in the epistemic setting may imply a higher computational cost due to additional grid levels, whereas the representation accuracy is preserved.

The local optimisations rely on finite differences to compute the first- and second-order derivative information. When sampling is employed to compute Equation (35), the sampling grid is kept constant within one major NLP iteration to avoid introducing noise in the computation of the objective's gradient and constraints' Jacobian.

In the following, we will present two approaches to the computation of the integrals in the two cases in which the distribution functions $p(\mathbf{z};\boldsymbol{\lambda})$ are explicitly available or not. In the former case we limit our attention to the treatment of Gaussian distributions $p(\mathbf{z};\boldsymbol{\lambda}) = \mathcal{N}(\mathbf{z};\boldsymbol{\lambda})$.

1. The Gaussian Case

In the Gaussian case the distribution of the uncertain parameters and initial conditions are Gaussians, and so are the distributions of the measurements:

$$\mathcal{X}_0 = \mathcal{N}\left(\mathbf{x}_0;\, \boldsymbol{\mu}_{X_0}, \boldsymbol{\Sigma}_{X_0}\right) \tag{36a}$$

$$\mathcal{D} = \mathcal{N}\left(\mathbf{d}\,;\, \boldsymbol{\mu}_{D}, \boldsymbol{\Sigma}_{D}\right) \tag{36b}$$

$$\mathcal{Y}_k = \mathcal{N}\left(\mathbf{y}_k|\mathbf{x}_k;\, \boldsymbol{\mu}_{Y_k}, \boldsymbol{\Sigma}_{Y_k}\right), \tag{36c}$$

where $\boldsymbol{\mu}_{(\cdot)}$ indicates the mean and $\boldsymbol{\Sigma}_{(\cdot)}$ the covariance of the normal distributions. The posterior distribution (23) at each stage k is generally not Gaussian. However, under certain conditions one can approximate the actual posterior with only the first two statistical moments [52] as it is commonly done in Kalman-type of sequential filters. Thus we can approximate the prior at stage k with:

$$\mathcal{X}_k^- = \sum_{j=1}^{M} b^{(j)} \mathcal{N}\left(\mathbf{x}_k\,;\, \boldsymbol{\mu}_{X_k^-}^{(j)}, \boldsymbol{\Sigma}_{X_k^-}^{(j)}\right) \tag{37}$$

with each mean and covariance given by

$$\begin{aligned}
\boldsymbol{\mu}_{X_k^-}^{(j)} &= \sum_{i=1}^{N} w^{(j,i)}\, \widetilde{F}_{k-1}^{k}(\boldsymbol{\xi}_{k-1}^{(j,i)}) \\
\boldsymbol{\Sigma}_{X_k^-}^{(j)} &= \sum_{i=1}^{N} w^{(j,i)} \left(\widetilde{F}_{k-1}^{k}(\boldsymbol{\xi}_{k-1}^{(j,i)}) - \boldsymbol{\mu}_{X_k^-}^{(j)}\right)\left(\widetilde{F}_{k-1}^{k}(\boldsymbol{\xi}_{k-1}^{(j,i)}) - \boldsymbol{\mu}_{X_k^-}^{(j)}\right)^T ,
\end{aligned} \tag{38}$$

where $\boldsymbol{\xi}_k^{(j,i)} = [\mathbf{x}_k^{(j,i)}, \mathbf{d}_k^{(j,i)}, \mathbf{u}_{e_k}^{(j,i)}]^T$ are the roots of the multivariate Hermite polynomial and $w^{(j,i)}$ the corresponding quadrature weights for the j-th belief component. The M observations $\mathbf{y}_k^{(j)}$ are sampled from the prior (37). The posterior

$$\mathcal{X}_k = \sum_{j=1}^{M} b^{(j)} \mathcal{N}\left(\mathbf{x}_k;\, \boldsymbol{\mu}_{X_k}^{(j)},\, \boldsymbol{\Sigma}_{X_k}^{(j)}\right) \tag{39}$$

is computed by updating the mean and the covariance matrix according to the observations received:

$$\begin{aligned} \boldsymbol{\mu}_{X_k}^{(j)} &= \boldsymbol{\mu}_{X_k^-}^{(j)} + \mathbf{K}_k(\mathbf{y}_k^{(j)} - \boldsymbol{\mu}_{Y_k}) \\ \boldsymbol{\Sigma}_{X_k}^{(j)} &= \boldsymbol{\Sigma}_{X_k^-}^{(j)} - \mathbf{K}_k \mathbf{S}_k \mathbf{K}_k^T \ . \end{aligned} \tag{40}$$

where the observation mean $\boldsymbol{\mu}_{Y_k}$ and Kalman gain $\mathbf{K}_k$ as

$$\begin{aligned} \boldsymbol{\mu}_{Y_k} &= \sum_{j=1}^{M} b^{(j)} \sum_{i=1}^{N} w^{(j,i)}\, h\big(\mathbf{x}_k^{(j,i)}, \boldsymbol{\varepsilon}_k^{(j,i)}\big) \\ \mathbf{S}_{Y_k} &= \sum_{j=1}^{M} b^{(j)} \sum_{i=1}^{N} w^{(j,i)} \big(h\big(\mathbf{x}_k^{(j,i)}, \boldsymbol{\varepsilon}_k^{(j,i)}\big) - \boldsymbol{\mu}_{Y_k}\big)\, \big(h\big(\mathbf{x}_k^{(j,i)}, \boldsymbol{\varepsilon}_k^{(j,i)}\big) - \boldsymbol{\mu}_{Y_k}\big)^T \\ \mathbf{C}_{XY_k} &= \sum_{j=1}^{M} b^{(j)} \sum_{i=1}^{N} w^{(j,i)} \big(\mathbf{x}_k^{(j,i)} - \boldsymbol{\mu}_{X_k}^-\big)\, \big(h\big(\mathbf{x}_k^{(j,i)}, \boldsymbol{\varepsilon}_k^{(j,i)}\big) - \boldsymbol{\mu}_{Y_k}\big)^T \\ \mathbf{K}_k &= \mathbf{C}_{XY_k}\, \mathbf{S}_{Y_k}^{-1} \ , \end{aligned} \tag{41}$$

with $\boldsymbol{\varepsilon}_k^{(j,i)}$ are realisations of the sensor noise, $\mathbf{S}_{Y_k}$ is the observation covariance, whereas $\mathbf{C}_{XY_k}$ is the cross covariance between state and observation. From the posterior, one can then compute the expectation of any function ϕ as

$$\mathbb{E}\big[\phi(\mathbf{X}_k) \,|\, \mathbf{y}_{1:k}\big] \approx \sum_{j=1}^{M} b^{(j)} \sum_{i=1}^{N} w^{(j,i)} \phi\big(\mathbf{x}_k^{(j,i)}\big) \ . \tag{42}$$

For ease of notation, the dependency on the control and parameter uncertainty has not been reported but the same form applies when ϕ depends on them by taking samples from their distributions as well.

The advantage of this approach over similar sample-based ones, e.g. Unscented Transform [53], is that the estimation fidelity can be made as accurate as desired simply using more quadrature points, that is a higher-order Hermite polynomial. A high accuracy computation of the integrals in Eq. (38) is made possible by the polynomial mapping $\widetilde{F}_{k-1}^k$, which can be employed to propagate a great number of samples inexpensively.

The multivariate Gauss-Hermite grid is usually constructed by Cartesian products of univariate ones. In order to alleviate the curse of dimensionality encountered in high-dimensional problems, like the ones tackled in navigation analysis, a sparse Gauss-Hermite version is employed to contain the number of samples for high stochastic dimensions [43].

2. General Distribution

When the posterior distribution at stage k cannot be easily expressed with an explicit function of the state variables, the prediction and update steps of the belief transition function, in Eq. (23), can be computed with the particle filter [51], a sequential Monte Carlo method that approximates the posterior density function as a discrete one by using samples $\mathbf{x}_k^{(i)}$, drawn from a proposal importance distribution $\pi\left(\mathbf{x}_k \,|\, \mathbf{x}_{k-1}, \mathbf{y}_{1:k}\right)$, as

$$\mathcal{X}_k^- = \sum_{j=1}^{M} b^{(j)} \sum_{i=1}^{N} w_k^{(i,j)}\, \delta\left(\mathbf{x}_k - \mathbf{x}_k^{(i,j)}\right) , \tag{43}$$

where $\delta(\cdot)$ is the Dirac function, $w_k^{(i,j)}$ and $\mathbf{x}_k^{(i,j)}$ are the i-th weight and sample to approximate the j-th belief component. In particle filters the propagation step is performed by drawing samples from a proposal distribution π as

$$\mathbf{x}_k^{(i,j)} \sim \pi\left(\mathbf{x}_k \,|\, \mathbf{x}_{k-1}^{(i,j)}, \mathbf{y}_{1:k}^{(j)}\right) , \tag{44}$$

which represent the prior discrete approximation. The proposal is chosen such that its support is larger than the posterior one. To construct the posterior approximation, the inference step is then carried out by updating the weights of the predicted samples as

$$w_k^{(i,j)} = w_{k-1}^{(i,j)}\, \frac{p(\,\mathbf{y}_k^{(j)} |\, \mathbf{x}_k^{(i,j)})\; p(\mathbf{x}_k^{(i,j)} |\, \mathbf{x}_{k-1}^{(i,j)})}{\pi\left(\mathbf{x}_k^{(i,j)} \,|\, \mathbf{x}_{k-1}^{(i,j)}, \mathbf{y}_{1:k}^{(j)}\right)} , \tag{45}$$

to account for the received observation $\mathbf{y}_k^{(j)}$ and the known dynamical evolution. The distribution $p(\mathbf{x}_k |\, \mathbf{x}_{k-1})$ is the state transition density describing the probabilistic evolution of the system due to uncertainty in $\mathbf{D}_{k-1}$. Once again, the conditional dependencies on the deterministic parameters have not been written down explicitly for ease of notation. Nonetheless, the proposal, transition and likelihood distributions could depend on them. The main motive behind the particle filter approach is that drawing samples directly from the posterior distribution is an unattainable task, whereas evaluating their density value is relatively easy thanks to Eq. (22). From the posterior in the form of Equation (43) one can then compute the expectation as

$$\mathbb{E}\left[\phi\left(\mathbf{X}_k\right) |\, \mathbf{y}_{1:k}\right] \approx \sum_{j=1}^{M} b^{(j)} \sum_{i=1}^{N} w_k^{(i,j)} \phi\left(\mathbf{x}_k^{(i,j)}\right) , \tag{46}$$

which is exactly the same as Eq. (42) but with weights and samples computed differently.

The accuracy of the discrete approximation and the particle filter performance greatly depend on the number of particles used, which is further critical for high-dimensional nonlinear problems like navigation analysis for space trajectory. Therefore, the polynomial mapping $\widetilde{F}_{k-1}^{k}$ constructed in the previous section results crucial in this scheme as it allows one to employ a larger number of samples, which can be propagated through an inexpensive polynomial

evaluation.

This particle filter-based approach to the practical computation of the shooting transcription should be employed in the most general case of non-Gaussian uncertainty, nonlinear dynamical system and observation model. This concludes the transcription method for the BOC as formulated in Eq. (16).

IV. Test Case: Europa Clipper Robust Optimisation

In this section, we apply BOC to the optimisation of one leg of the Europa Clipper tour [54]. The original tour comes from a deterministic design, however, from a navigation analysis, the leg of interest, labelled E17-E18, yields a dangerously high probability of impact with Europa at flyby E18. Such deterministic trajectory is used as initial guess for the robust optimisation. Therefore, the goal of this test case is to re-optimise the E17-E18 open-loop trajectory with BOC so that the flight dynamics requirements are satisfied and the remainder of the tour remains feasible. The problem is to minimise the sum of deterministic and statistical manoeuvres while respecting the constraints on the desired B-plane flyby parameter **b**, the hyperbolic Time of Closest Approach (TCA) [55], the expected value of the final position, and a constraint on the collision probability with Europa. We will study both the case of purely aleatory uncertainty and the case of mixed aleatory and epistemic uncertainty.

The scenario addressed is this section is depicted in Figs. 3. Each subplot in Figs. 3 represents a phase of the

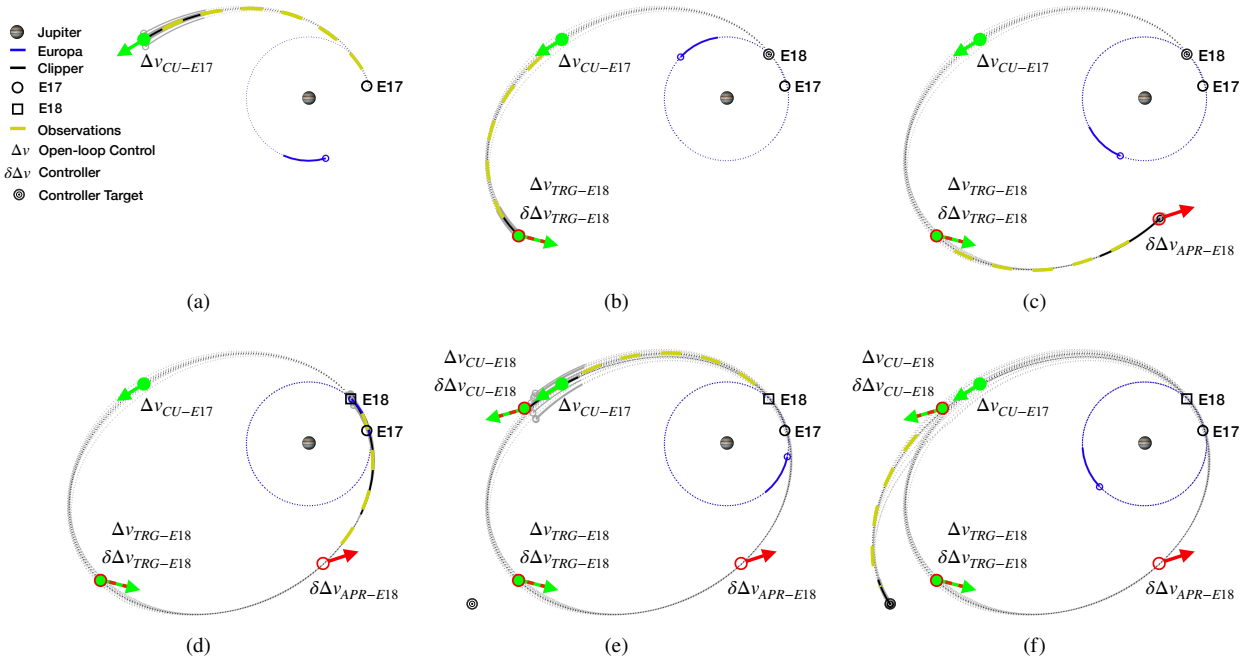

Fig. 3 Schematic representation of navigation analysis setup for part of Europa Clipper leg belief optimisation test case.

analysed trajectory, specifically:

(a) The $E17 - CU\text{-}E17$ phase (Fig. 3(a)) starts from the initial belief $\mathcal{X}_0$, and goes till the first control point, 3 days after $E17$, denoted as Clean-Up (CU).

(b) The $CU\text{-}E17 - TRG\text{-}E18$ phase (Fig. 3(b)) starts from the CU, where the belief state is given by the ensemble $\sum_j b_j p_j$, executes the open-loop manoeuvre $\Delta\bar{\mathbf{v}}_{CU\text{-}E17}$ and propagates till the next control point near the trajectory apocenter, approximately 6 days later, denoted as Targeting (TRG).

(c) The $TRG\text{-}E18 - APR\text{-}E18$ phase (Fig. 3(c)) starts from TRG with the belief state given by the ensemble $\sum_j b_j p_j$, performs manoeuvre $\Delta\bar{\mathbf{v}}_{TRG\text{-}E18} + \delta\Delta\mathbf{v}_{TRG\text{-}E18}$ and propagates till the pre-flyby control point, 3 days before flyby, denoted as Approach (APR).

(d) The $APR\text{-}E18 - E18$ phase (Fig. 3(d)) starts from APR with the belief state given by the ensemble $\sum_j b_j p_j$, performs the feedback manoeuvre $\delta\Delta\mathbf{v}_{APR\text{-}E18}$ and extends till flyby $E18$.

(e) The $E18 - CU\text{-}E18$ phase (Fig. 3(e)) starts from $E18$ with the belief state given by the ensemble $\sum_j b_j p_j$, extends till the successive clean-up point $CU\text{-}E18$, 3 days after the flyby.

(f) The $CU\text{-}E18 - T_F$ phase (Fig. 3(f)) starts from T_F with the belief state given by the ensemble $\sum_j b_j p_j$, performs manoeuvre $\Delta\bar{\mathbf{v}}_{APR\text{-}E18} + \delta\Delta\mathbf{v}_{CU\text{-}E18}$ and extends till the leg final time, 7 days after the flyby.

During each phase, OD campaigns are carried out, represented in yellow, with an 8 hours ON 8 hours OFF schedule (dashed line) to improve the knowledge of the trajectory. The 8 hours ON 8 hours OFF is the access schedule of the Deep Space Network (DSN) for Europa Clipper, with range and range-rate measurements generally employed, whereas Delta-DOR is used only when specifically needed. Therefore, this latter measurement type will not be included in the observation model. The OD stops at a cut-off time before the subsequent manoeuvre, here set to one day, to model the time needed by the operators to compute the updated trajectory. The aforementioned polynomial NA approach is employed to simulate observation samples and update the belief state.

The Probability of Impact (PoI) with Europa is computed by propagating the belief state after the targeting manoeuvre $\Delta\bar{\mathbf{v}}_{TRG\text{-}E18} + \delta\Delta\mathbf{v}_{TRG\text{-}E18}$ to the nominal flyby time without applying the successive approach manoeuvre $\delta\Delta\mathbf{v}_{APR\text{-}E18}$ or performing additional OD. This mapped uncertainty projected onto the B-plane is computed by applying map $\mathcal{T}_P$ only. A constraint on the PoI is then enforced to ensure environmental protection to Europa even in the event of spacecraft loss after the main manoeuvre.

The whole trajectory lasts for 21 days, from E17 to the second apocenter passage. The trajectory in Fig. 3 is defined in an inertial reference frame, mean equinox and ecliptic of J2000 (ECLIPJ2000) [56], centered in Jupiter. This frame has the $\hat{\mathbf{x}}$ axis pointing to the mean vernal equinox at January 1, 2000, the $\hat{\mathbf{z}}$ axis normal to the ecliptic plane, and $\hat{\mathbf{y}}$ completing the right-handed frame. The spacecraft motion $\mathbf{x}(t)$ is governed by a high-fidelity full-ephemeris dynamics, taking into account the gravitational field of Jupiter (central and J_2 effects), of its moons Europa (central and J_2), Io, Ganymede and Callisto, and of the Sun. The dynamics is integrated with the propagation module of the trajectory optimisation tool jTOP [3]. This black-box module has been used to propagate collocation points to train the

non-intrusive surrogate model described in Section III.B. The outer and inner optimisation loops are solved with two nested instances of the local solver MATLAB *fmincon*.

In this section, we will talk about delivered and mapped uncertainty. By delivered uncertainty, we intend the output of pure dynamical propagation of the belief state in time without further OD. By mapped uncertainty, we intend the output of a generic transformation of the belief state, e.g. conversion to B-plane parameters.

A. Problem Definition

For this application, the interest is in finding the optimal *open-loop* control $\Delta\overline{\mathbf{v}}$ which yields the most robust and reliable trajectory under uncertainty in navigation analysis and manoeuvre execution errors. Hence, the executed control $\mathbf{U}_e$ acting on the belief components is written as

$$\Delta\mathbf{V}_e(t_k, \mathbf{X}_k) = \Delta\overline{\mathbf{v}}(t_k) + \delta\Delta\mathbf{v}(\mathbf{X}_k^{(j)}) + \boldsymbol{\Theta}\big(\Delta\overline{\mathbf{v}}(t_k) + \delta\Delta\mathbf{v}(\mathbf{X}_k^{(j)}), \boldsymbol{\lambda}_k\big) \,, \tag{47}$$

where the open-loop nominal impulse $\overline{\mathbf{u}} = \Delta\overline{\mathbf{v}}(t_k)$ is to be optimised and the disturbance $\boldsymbol{\Theta}$ depends nonlinearly on the commanded control $\Delta\mathbf{v} = \Delta\overline{\mathbf{v}}(t_k) + \delta\Delta\mathbf{v}(\mathbf{X}_k^{(j)})$. The definition of $\boldsymbol{\Theta}$ follows the Gates' model [57, 58] (see Figure 4). In this model the disturbance is defined in terms of modulus and angular variations on the commanded $\Delta\mathbf{v}$. In a frame centred in the spacecraft with the z-axis aligned with $\Delta\mathbf{v}$, the y-axis perpendicular to both the $\Delta\mathbf{v}$ and the ecliptic normal, and the x-axis completing the right-handed frame, the execution error components are taken from zero-mean normal distributions

$$\begin{aligned} \Theta_x &\sim \mathcal{N}(0, \sigma_{pf}^2 + \sigma_{pp}^2 \Delta v) \\ \Theta_y &\sim \mathcal{N}(0, \sigma_{pf}^2 + \sigma_{pp}^2 \Delta v) \\ \Theta_z &\sim \mathcal{N}(0, \sigma_{mf}^2 + \sigma_{mp}^2 \Delta v) \,, \end{aligned} \tag{48}$$

where Δv is the magnitude of $\Delta\mathbf{v}$, σ_{mf} and σ_{mp} are respectively the standard deviations of the fixed and proportional magnitude component, while σ_{pf} and σ_{pp} concern the pointing components. In this model, the pointing error is decomposed into two components in the plane normal to the commanded $\Delta\mathbf{v}$, which is equivalent to decomposing it in terms of magnitude and angular components for suitable distributions [58].

These three components are then rotated into the inertial reference frame in which $\Delta\mathbf{v}$ is defined to yield the vector $\boldsymbol{\Theta}$. The components of the parameters vector $\boldsymbol{\lambda}_k = [\sigma_{mf}, \sigma_{mp}, \sigma_{pf}, \sigma_{pp}]^T$ have crisp values for the pure aleatory case, as defined in Table 1, whereas they are interval-valued for the epistemic case, as in Table 2. Errors in the execution time of the manoeuvres are not explicitly accounted for in this model.

The closed-loop control component $\delta\Delta\mathbf{v}(\mathbf{X}_k^{(j)})$ is an analytical linear function from time t_k to a generic target state at time $t_\circledcirc$, which therefore needs not to coincide with the end of that segment t_{k+1}. Let $\mathbf{x} = [\mathbf{r}, \mathbf{v}]$ be the decomposition of

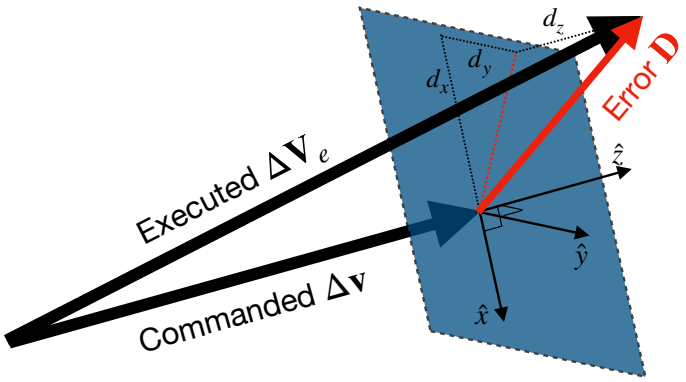

Fig. 4 Execution error by Gates' model.

the spacecraft inertial state in position and velocity. The linear guidance law to target the position $\mathbf{r}_\oslash$ is computed as follows. First, the dynamics is linearised around the nominal trajectory in $[t_k, t_\oslash]$, that is the one computed using only the optimisable open-loop control $\Delta\bar{\mathbf{v}}$, to obtain a linear mapping

$$\begin{bmatrix} \delta\mathbf{r}_\oslash \\ \delta\mathbf{v}_\oslash \end{bmatrix} = \Phi_k^\oslash \begin{bmatrix} \delta\mathbf{r}_k \\ \delta\mathbf{v}_k + \delta\Delta\mathbf{v}_k \end{bmatrix} = \begin{bmatrix} \Phi_{k\,1,1}^\oslash & \Phi_{k\,1,2}^\oslash \\ \Phi_{k\,2,1}^\oslash & \Phi_{k\,2,2}^\oslash \end{bmatrix} \begin{bmatrix} \delta\mathbf{r}_k \\ \delta\mathbf{v}_k + \delta\Delta\mathbf{v}_k \end{bmatrix} , \tag{49}$$

where the Cartesian state deviation $\delta\mathbf{x}_k$ has been decomposed in position $\delta\mathbf{r}_k$ and velocity $\delta\mathbf{v}_k$ deviations, and $\Phi_k^\oslash$ has been accordingly partitioned in 3×3 blocks. The linear guidance is obtained by imposing

$$\delta\mathbf{r}_\oslash = \mathbf{0}$$

which leads to

$$\delta\Delta\mathbf{v}_k = -\Phi_{k\,1,2}^{\oslash\,-1} \begin{bmatrix} \Phi_{k\,1,1}^\oslash & \Phi_{k\,1,2}^\oslash \end{bmatrix} \begin{bmatrix} \delta\mathbf{r}_k \\ \delta\mathbf{v}_k \end{bmatrix} . \tag{50}$$

This guidance law is employed for the controller $\delta\Delta\mathbf{v}_{CU\text{-}E18}$ to target the final nominal position.

The targeting and approach manoeuvres, respectively $\delta\Delta\mathbf{v}_{TRG\text{-}E18}$ and $\delta\Delta\mathbf{v}_{APR\text{-}E18}$, target the B-plane parameters instead [55]. Let $\mathbf{B}_\oslash = [\mathbf{b}_\oslash, \mathrm{TCA}_\oslash]$ be the B-plane parameters targeted, with $\mathbf{b}$-vector expressed in two components ($b_t = \mathbf{b} \cdot \hat{\mathbf{t}}$ and $b_r = \mathbf{b} \cdot \hat{\mathbf{r}}$) and TCA being the hyperbolic time of closest approach, $\mathcal{B}$ the corresponding coordinate transformation from the inertial state $\mathbf{B} = \mathcal{B}(\mathbf{x})$, and $\mathbf{J}_\mathcal{B}$ its Jacobian (see Appendix A). Using the linearisation as above,

the deviations in B-plane parameters from the nominal ones are written as

$$\delta\mathbf{B}_{\circledcirc} = \mathbf{J}_{\mathcal{B}}\,\Phi^{\circledcirc}_{k}\begin{bmatrix}\delta\mathbf{r}_k\\ \delta\mathbf{v}_k+\delta\Delta\mathbf{v}_k\end{bmatrix} = \begin{bmatrix}\partial\mathbf{B}/\partial\mathbf{r}_{\circledcirc} & \partial\mathbf{B}/\partial\mathbf{v}_{\circledcirc}\end{bmatrix}\begin{bmatrix}\Phi^{\circledcirc}_{k\,1,1} & \Phi^{\circledcirc}_{k\,1,2}\\ \Phi^{\circledcirc}_{k\,2,1} & \Phi^{\circledcirc}_{k\,2,2}\end{bmatrix}\begin{bmatrix}\delta\mathbf{r}_k\\ \delta\mathbf{v}_k+\delta\Delta\mathbf{v}_k\end{bmatrix} \quad . \tag{51}$$

By imposing

$$\delta\mathbf{B}_{\circledcirc} = \mathbf{0}$$

and by matrix manipulation, the B-plane targeting is obtained as a linear guidance law as

$$\delta\Delta\mathbf{v}_k = -\left(\frac{\partial\mathbf{B}}{\partial\mathbf{r}_{\circledcirc}}\Phi^{\circledcirc}_{k\,1,2}+\frac{\partial\mathbf{B}}{\partial\mathbf{v}_{\circledcirc}}\Phi^{\circledcirc}_{k\,2,2}\right)^{-1}\mathbf{J}_{\mathcal{B}}\,\Phi^{\circledcirc}_{k}\begin{bmatrix}\delta\mathbf{r}_k\\ \delta\mathbf{v}_k\end{bmatrix} . \tag{52}$$

This guidance law is employed for the controllers $\delta\Delta\mathbf{v}_{TRG\text{-}E18}$ and $\delta\Delta\mathbf{v}_{APR\text{-}E18}$ to target the nominal B-plane parameters. Hence, the belief component-dependent controller $\delta\Delta\mathbf{v}(\mathbf{X}_k^{(j)})$ employed in this test case is computed according to either Eq. (50) or (52) depending on the targeted parameters. The quantities $\delta\mathbf{r}_k$ and $\delta\mathbf{v}_k$ are the deviations of the belief component expected value $\mathbb{E}\big[\mathbf{X}_k^{(j)}\big]$ with respect to the nominal trajectory at time t_k.

As for the orbit determination campaigns, the measured quantity is the range and range-rate of the spacecraft with respect to Earth (see Sections 3.2.1-3.2.2 in [40]). The likelihood function is modelled as Gaussian, and the associated covariance characterising the observation accuracy is assumed diagonal (see Table 1).

Once the execution and navigation errors are defined we can explicitly write the BOC formulation as follows:

$$\min_{\Delta\bar{\mathbf{v}}_i}\ \Delta v99 \tag{53a}$$

$$\text{s.t.}\quad \mathcal{X}_k = \mathcal{T}\left(\mathcal{X}_{k-1},\,\mathcal{D}_{k-1},\,\Delta\mathcal{V}_{e_{k-1}},\,\mathcal{E}_k\right) \tag{53b}$$

$$\underline{P}\left(\|\Delta\mathbf{V}_{e_{tot}}\| < \Delta v99\right) = .99 \tag{53c}$$

$$\overline{\text{PoI}} < \varepsilon \tag{53d}$$

$$\underline{\mathbb{E}}\big[\mathbf{B}_{E18}\big],\,\overline{\mathbb{E}}\big[\mathbf{B}_{E18}\big] \in \mathbf{\Phi}_{\mathbf{B}_{E18}} \tag{53e}$$

$$\underline{\mathbb{E}}\big[\mathbf{R}_F\big],\,\overline{\mathbb{E}}\big[\mathbf{R}_F\big] \in \mathbf{\Phi}_{\mathbf{R}_F} \tag{53f}$$

$$\mathcal{X}_0 \in \mathcal{P}_{x_0}\,,\,\theta \in \mathcal{P}_{\mathbf{\Theta}}\,,\,\mathcal{Y}_k = \mathcal{N}_{\mathbf{Y}_k|\mathbf{X}_k}\left(\boldsymbol{\mu}_{y_k},\mathbf{\Sigma}_{y_k}\right), \tag{53g}$$

where k denotes the time discretisation with multiple arcs which can contain both control and observations, only control, only observations or neither of the two according to the phases described in Figs. 3. The objective to be minimised is the threshold value $\Delta v99$ on the quantile of the magnitude of the total $\|\Delta\mathbf{V}_{e_{tot}}\|$. Eq. (53c) expresses the quantile with a

constraint on the lower probability P that the total cost is below the threshold $\Delta v99$ (see (9) for the expression of P). The total magnitude $\|\Delta\mathbf{V}_{e_{tot}}\|$ including execution errors is defined as:

$$\|\Delta\mathbf{V}_{e_{tot}}\| = \sum_i \|\Delta\mathbf{V}_{e_i}(t_k, \mathbf{X}_k)\| + \|\Delta\mathbf{V}_F\|$$

which is a random variable encompassing all manoeuvres (indexed by $i \in \{CU\text{-}E17, TRG\text{-}E18, APR\text{-}E18, CU\text{-}E18\}$) plus the final velocity mismatch magnitude $\|\Delta\mathbf{V}_F\| = \|\mathbf{V}_F - \overline{\mathbf{v}}_F\|$ between the final state velocity and the original final velocity. Numerically, this constraint is computed with Equation (42) using $\phi = \mathbb{1}_{\|\Delta\mathbf{v}_{e_{tot}}\|<\Delta v99}$ by taking samples from the executed control distribution $\Delta\mathcal{V}_e$ and the final velocity mismatch $\Delta\mathcal{V}_F$. In particular for the latter, samples $\mathbf{x}_F^{(i)}$ are first generated from the final belief state $\mathcal{X}_F$, then the velocity vector of each sample $\mathbf{v}_F^{(i)}$ is subtracted by the target final velocity $\overline{\mathbf{v}}_F$, and finally the norm of this difference is used as a sample of the velocity mismatch magnitude. Constraint (53f) imposing the expected value of the final position vector, together with the mismatch $\|\Delta\mathbf{V}_F\|$ in the objective function, ensures that the expectation of the $E17 - E18$ trajectory connects with the remainder of the original tour.

Eq. (53b) is the belief transition function from segment k to segment $k+1$. The transition function incorporates the effect of observations and manoeuvres, when present within a segment.

Eq. (53d) is the upper bound on the probability of impact $\overline{\text{PoI}}$ after targeting and it is written as the upper bound on the probability of the minimum distance from Europa, at flyby E18, to be smaller or equal to the radius of Europa written as

$$\text{PoI} = \int \mathbb{1}_{\phi(\mathbf{x}_{E18})\leq R_{EUR}}(\mathbf{x}_{E18})\, p(\mathbf{x}_{E18}; \boldsymbol{\lambda})\, d\mathbf{x}_{E18}\,, \tag{54}$$

where $r_{E18} = \phi(\mathbf{x}_{E18})$ is the function mapping the Cartesian state at $E18$ to the pericenter distance of the hyperbolic trajectory with respect to Europa. This probability is constrained to be less than $\varepsilon = 0.1\%$. Numerically, this constraint is computed using eq. (42) with $\phi = \mathbb{1}_{r_{E18}\leq R_{EUR}}$.

Eq. (53e) imposes the expected values of the B-plane flyby conditions to be within a target set $\boldsymbol{\Phi}_{\mathbf{B}_{E18}}$. In the first test case with purely aleatory uncertainty, the set is a singleton composed of the target B-parameter $\boldsymbol{\Phi}_{\mathbf{B}_{E18}} = \{\widehat{\mathbf{B}}\}$. In the second case with epistemic uncertainty, the target set is defined as an hyperbox around the target value $\widehat{\mathbf{B}} = [\widehat{b}_t, \hat{b}_r, \widehat{\text{TCA}}]$ as

$$\boldsymbol{\Phi}_{\mathbf{B}_{E18}} = [\hat{b}_t - \delta b_t, \hat{b}_t + \delta b_t] \times [\hat{b}_r - \delta b_r, \hat{b}_r + \delta b_r] \times [\widehat{\text{TCA}} - \delta\,\text{TCA}, \widehat{\text{TCA}} + \delta\,\text{TCA}] \tag{55}$$

where the tolerances are set to $\delta b_t = 0.5$ [km], $\delta b_r = 0.5$ [km] and $\delta\,\text{TCA} = 0.05$ [s].

Similarly, Eq. (53f) requires the lower and upper expectations of the final position to be within the set $\boldsymbol{\Phi}_{\mathbf{R}_F}$. In the aleatory case, the set is composed of a single element $\boldsymbol{\Phi}_{\mathbf{R}_F} = \{\hat{\mathbf{r}}_F\}$. In the epistemic case, the set is defined as a

hyper-box around the precise target position as

$$\mathbf{\Phi}_{\mathbf{R}_F} = [\hat{\mathbf{r}}_{F_x} - \delta\mathbf{r}_{F_x}, \hat{\mathbf{r}}_{F_x} + \delta\mathbf{r}_{F_x}] \times [\hat{\mathbf{r}}_{F_y} - \delta\mathbf{r}_{F_y}, \hat{\mathbf{r}}_{F_y} + \delta\mathbf{r}_{F_y}] \times [\hat{\mathbf{r}}_{F_z} - \delta\mathbf{r}_{F_z}, \hat{\mathbf{r}}_{F_z} + \delta\mathbf{r}_{F_z}] \tag{56}$$

for the $x-$, $y-$ and $z-$components of the position vector and where each tolerance is $\delta\mathbf{r}_{F_{(\cdot)}} = 10$ km because variations in the next apocenter position are less critical and can be compensated with successive manoeuvres. In the epistemic case, these constraints imply that the open-loop optimum under uncertainty needs to satisfy, in expectation, the flyby and terminal conditions within a set for all distributions in the imprecise set $\mathcal{P}_\lambda$.

Finally, Eqs.(53g) define the initial belief condition, the uncertain parameters distribution and the observation likelihood.

For comparison, the dOCP for the first guess generation optimises only the nominal Δv while respecting the reference initial conditions, flyby B-plane parameters $\widehat{\mathbf{B}}$, and final boundary conditions $\hat{\mathbf{r}}_F$. No observations are employed in the deterministic first guess generation.

In the pure aleatory case, the epistemic sets are composed of a single distribution each, that is $\mathcal{P}_{x_0} = \left\{\mathcal{N}\left(\boldsymbol{\mu}_{x_0}, \mathbf{\Sigma}_{x_0}\right)\right\}$ and $\mathcal{P}_{\mathbf{\Theta}} = \{p(\boldsymbol{\theta}; \boldsymbol{\lambda}_{\mathbf{\Theta}})\}$ is described by a single Gates' model distribution as described above. The parameters for these uncertainty models are reported in Table 1. These values come from previous navigation analysis studies for Europa Clipper [49, 59]. The table reports respectively the square root of the diagonal values (standard deviations) for the initial dispersion covariance $\mathbf{\Sigma}_{x_0}$, with typical values reconstructed from OD campaigns post-flyby, the Gates' model parameters $\boldsymbol{\lambda}_{\mathbf{\Theta}}$ for the execution errors, and the standard deviation values for the accuracy of each observation type $\mathbf{\Sigma}_{y_k}$. The initial mean $\boldsymbol{\mu}_{x_0}$ is the spacecraft initial state coming from the deterministic tour design used as initial guess.

In the epistemic scenario, we consider the following uncertainty components. The initial dispersion considered in the aleatory scenario is the reconstructed uncertainty from simulated OD arcs post-flyby. Therefore, the values in Table 1 are estimated during the navigation analysis in the mission design phase, whereas the actual dispersion to consider during operations may vary from these values. This further uncertainty is modelled as epistemic, and the imprecise initial set is parameterised as

$$\begin{aligned}\mathcal{P}_{x_0} = \{\, p(\mathbf{x}_0) :\ & p(\mathbf{x}_0) = \mathcal{N}\left(\mathbf{x}_0; \boldsymbol{\mu}_{x_0}, \tilde{\mathbf{\Sigma}}_{x_0}\right), \\ & \tilde{\mathbf{\Sigma}}_{x_0} = \text{blkdiag}(\, \lambda_{x_{0-1}}\, \mathbf{\Sigma}_{x_0}(1{:}3, 1{:}3),\ \lambda_{x_{0-2}}\, \mathbf{\Sigma}_{x_0}(4{:}6, 4{:}6)), \\ & \lambda_{x_{0-1}} \in [0.5, 2.0],\ \lambda_{x_{0-2}} \in [0.5, 2.0] \,\}\,,\end{aligned} \tag{57}$$

where $\mathbf{\Sigma}_{x_0}(1{:}3, 1{:}3)$ and $\mathbf{\Sigma}_{x_0}(4{:}6, 4{:}6)$ indicate respectively the position block and the velocity block, the operator blkdiag indicates a block-diagonal matrix, $\lambda_{x_{0-1}}$ and $\lambda_{x_{0-2}}$ are two multipliers scaling the precise covariance matrix $\mathbf{\Sigma}_{x_0}$ defined from the standard deviations in Table 1. Being the multipliers defined within $[0.5, 2.0]$, they encompass distributions

with covariance from half up to double the magnitude of the pure aleatory one. That is, the epistemic multipliers can give more or less confidence to the initial state knowledge. For the execution errors, the epistemic set $\mathcal{P}_{\boldsymbol{\Theta}} = \left\{p(\boldsymbol{\theta}; \tilde{\boldsymbol{\lambda}}_{\boldsymbol{\Theta}})\right\}$ is constructed by allowing interval-valued parameters $\tilde{\boldsymbol{\lambda}}_{\boldsymbol{\Theta}}$ in the Gates' model. Indeed, these parameters are estimated by testing the engine in nonoperational conditions and then updated multiple times during the spacecraft operational life with possible substantial changes, as it happened, for example, during the Cassini mission [60]. Specifically, the intervals for the model parameters considered in the epistemic analysis are reported in Table 2, which include the precise values employed in the pure aleatory scenario. For missions like Europa Clipper, the observations from Earth are generally performed from the DSN. In such advanced facilities, the instruments and operating conditions are well known and precisely controlled. Therefore, the likelihood distribution describing the observation noise is well characterised. Hence, the zero-mean observation errors are assumed to remain purely aleatory also in the case of epistemic uncertainty on initial conditions and manoeuvre execution. Nonetheless, the overall OD remains an epistemic process because the priors, resulting from the initial conditions and execution errors, are epistemic.

Other model uncertainty sources are not included in this preliminary test case, e.g. celestial bodies' ephemerides uncertainty, although they may be relevant for a complete navigation analysis.

Table 1 Parameters of aleatory uncertainty models considered in Europa's moon flyby belief optimisation.

Uncertainty	Component	Value	
Initial Dispersion	1σ Position (RTN)	[3.7, 5.3, 9.3]	[m]
	1σ Velocity (RTN)	[2.3, 3.4, 5.9]	[mm/s]
Execution Error	Fixed Pointing σ_{pf}	3.33	[mm/s]
	Proportional Pointing σ_{pp}	6.67	[mrad]
	Fixed Magnitude σ_{mf}	4.67	[mm/s]
	Proportional Magnitude σ_{mp}	0.33%	[-]
Observation Accuracy	1σ Range	3.0	[m]
	1σ Range-rate	0.1	[mm/s]

Table 2 Interval-valued epistemic parameters for initial covariance multipliers and Gates' parameters in Europa's moon flyby belief optimisation.

Uncertainty	Component	Value	
Initial Dispersion	Position multiplier $\lambda_{x_{0-1}}$	[0.5, 2.0]	[-]
	Velocity multiplier $\lambda_{x_{0-2}}$	[0.5, 2.0]	[-]
Execution Error	Fixed Pointing $\tilde{\sigma}_{pf}$	[1.67, 4.00]	[mm/s]
	Proportional Pointing $\tilde{\sigma}_{pp}$	[3.33, 8.00]	[mrad]
	Fixed Magnitude $\tilde{\sigma}_{mf}$	[2.33, 6.60]	[mm/s]
	Proportional Magnitude $\tilde{\sigma}_{mp}$	[0.17, 0.40]%	[-]

B. Results

This section presents the results of the belief optimisation, first under aleatory uncertainty only, then under the complete mixed aleatory and epistemic uncertainty model. The simulations were performed in Matlab R2020b on macOS Big Sur 3.5GHz Dual-Core i7.

1. Aleatory uncertainty

First, we analyse the case of purely aleatory uncertainty. We start from the deterministic optimal initial guess reported in Table 3, which was computed by optimising the nominal trajectory with the open-loop control only. This solution meets the flyby and final position constraints but violates the required probability of impact with the moon when a navigation analysis is performed. In fact, the probability of impact is PoI = 0.75% $\not\leq$ 0.1%. A visualization

Table 3 Free variables, open-loop magnitude $\Delta\overline{v}$, total $\Delta v99$, their ratio and PoI for first guess under aleatoric uncertainty.

Solution	Aleatory First Guess
$\Delta\mathbf{v}_{CU\text{-}E17}$ [m/s]	[0.0 , 0.0 , 0.0]
$\Delta\mathbf{v}_{TRG\text{-}E18}$ [m/s]	[−1.30, +2.86, +3.23]
$\Delta\mathbf{v}_{CU\text{-}E18}$ [m/s]	[0.0 , 0.0 , 0.0]
$\Delta\overline{v}$ [m/s]	4.51
$\Delta v99$ [m/s]	8.05
$\Delta v99/\Delta\overline{v}$ [-]	1.79
PoI [-]	0.75%

of the probability of impact for this solution is displayed in Fig. 5, where the state uncertainty at different times along the trajectory is propagated onto the B-plane of the Europa flyby E18, without applying successive manoeuvres or performing any new orbit determination campaign. Different samples drawn from the belief state distribution have different velocity vectors resulting in different incoming asymptotes which, in turn, result in different B-plane orientations. In this paper, the mapping of the uncertainty onto the B-plane coordinates is realised by letting the B-plane frame vary for each sample as suggested in [61] for collision scenarios. Hence, Fig. 5 employs a single plane for representing all the B-parameters resulting from different state realisations, although their corresponding B-planes are different. Thus, the confidence ellipses are reconstructed from the mapped $\mathbf{b}-$vector samples, each of which has a different reference frame.

Fig. 5(a) shows the ellipses that would result on the B-plane if the spacecraft was not controlled or observed anymore after the E17 clean-up. Fig. 5(b) shows the ellipse of uncertainty on the B-plane propagated from the TRG (see Fig. 3(b)). The figure shows that without corrections coming from a navigation analysis the uncertainty on this deterministic

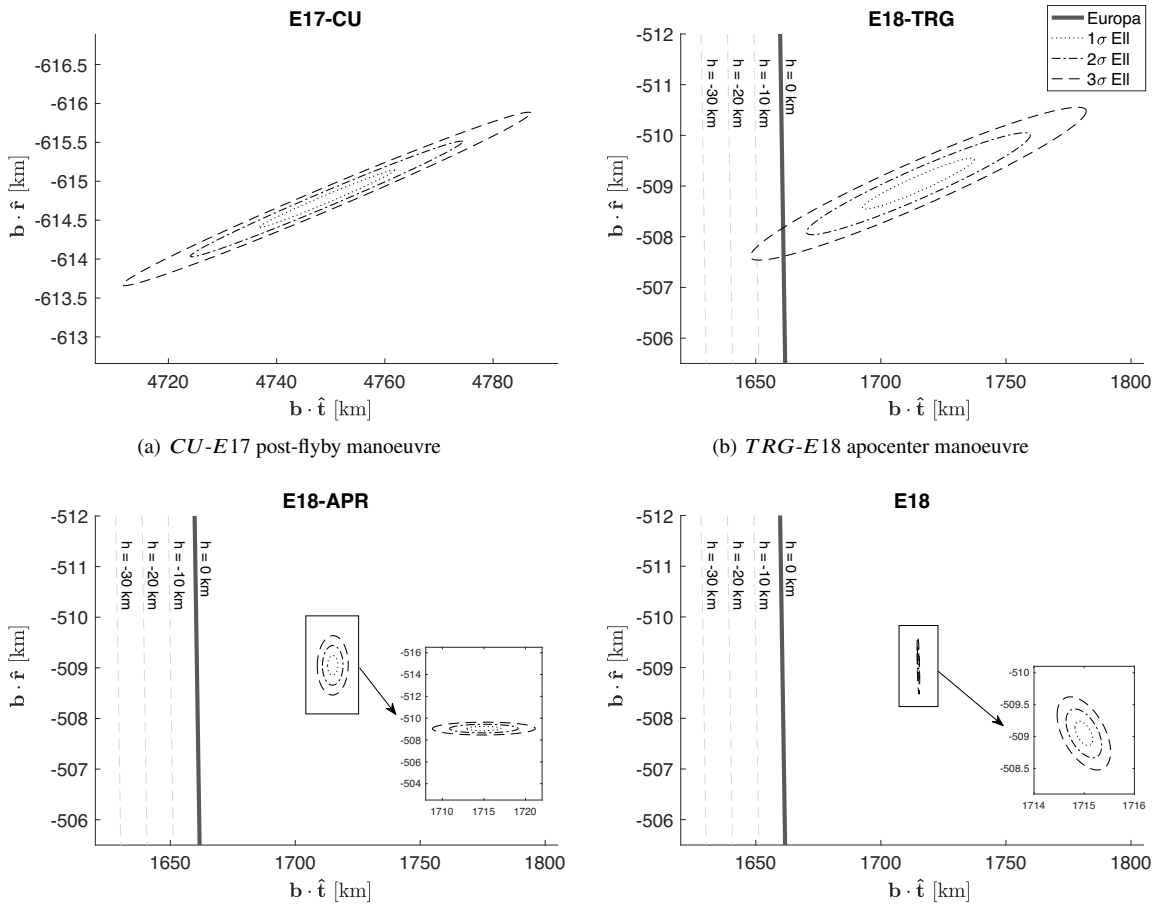

(a) CU-$E17$ post-flyby manoeuvre

(b) TRG-$E18$ apocenter manoeuvre

(c) APR-$E18$ approach manoeuvre

(d) $E18$ closest approach

Fig. 5 Confidence ellipses in B-vector components mapped from different instances of the first guess trajectory without successive manoeuvres and observations under aleatory uncertainty.

trajectory has an intersection with the surface of the moon (represented by the thick black line at $h = 0$ km), which corresponds to an undesirably high PoI. Fig. 5(c) displays the B-plane uncertainty propagated without new OD after the APR (see also Fig. 6(c)), which is notably smaller than the post-targeting one because of the new OD arcs and the controller $\delta\Delta\mathbf{v}_{APR\text{-}E18}$. Fig. 5(d) finally shows the uncertainty on the B-plane as reconstructed using the OD arcs after the APR. The estimated overall $\Delta v99$ is approximately 79% larger than the open-loop one (see Table 3), a cost increase in line with previous navigation analysis for the Europa Clipper trajectory [48].

We now apply BOC, starting from the deterministic solution, to find a trajectory that minimises the $\Delta v99$ while respecting the $\overline{\text{PoI}}$ constraint, and satisfying the constraints on the flyby conditions and terminal position. The resulting solution fulfils the constraint on the probability of impact. A summary of its characteristics is reported in Table 4. The average wall time for computing this BOC trajectory is slightly above 3 minutes.

Looking at the open-loop $\Delta\bar{\mathbf{v}}$ allocation, one can infer that the feasibility on the PoI constraint was realised by trading off part of the targeting manoeuvre with the clean-up ones. The execution errors coming from an increased $\Delta\bar{\mathbf{v}}_{CU\text{-}E17}$

Table 4 Free variables, open-loop magnitude $\Delta\overline{v}$, total $\Delta v99$, their ratio and PoI for robust solution under aleatoric uncertainty.

Solution	Aleatory Robust
$\Delta\overline{\mathbf{v}}_{CU\text{-}E17}$ [m/s]	$[+0.12, +0.18, +0.09]$
$\Delta\overline{\mathbf{v}}_{TRG\text{-}E18}$ [m/s]	$[-2.09, +2.01, +1.99]$
$\Delta\overline{\mathbf{v}}_{CU\text{-}E18}$ [m/s]	$[-1.21, +0.56, -1.79]$
$\Delta\overline{v}$ [m/s]	5.98
$\Delta v99$ [m/s]	9.91
$\Delta v99/\Delta\overline{v}$ [-]	1.66
PoI [-]	0.09‰

can be adjusted by the controller at the apocenter, while the smaller $\Delta\overline{\mathbf{v}}_{TRG\text{-}E18}$ and associated execution errors result in a smaller uncertainty at the flyby B-plane (see Fig. 6(b)). After the flyby, a $\Delta\overline{\mathbf{v}}_{CU\text{-}E18}$ manoeuvre is needed to meet the target conditions at the final time.

Overall the optimal trajectory has a higher open-loop magnitude $\Delta\overline{v}$ than the first guess, but the feasibility is restored. We observe that the percentage increase of the $\Delta v99$, with respect to the open-loop $\Delta\overline{v}$, is now lower, i.e. 66%, indicating that the BOC trajectory can compensate for the possible uncertainty realisations more efficiently. Fig. 6 shows the B-plane uncertainties of the robust trajectory. Fig. 6(b), representing the uncertainty mapped after TRG, shows that the 3-σ ellipse does not cross the surface of Europa anymore. By comparing it with the corresponding plot in Figure 5(b), the robust B-plane ellipse has a smaller semi-major axis, which mainly contributes to the PoI, whereas it has a larger semi-minor axis, which has a limited contribution to the PoI constraint. The robust ellipse is also rotated counterclockwise, which leads to an even lower impact probability.

To quickly verify that the increase in total $\Delta v99$ between the robust solution and the first guess is due to the initial infeasibility, the BOC problem has been solved after removing the PoI constraint. Table 5 shows the unconstrained optimal solution, which displays a lower overall $\Delta v99$ compared to that of the deterministic solution, although the open-loop magnitude $\Delta\overline{v}$ is slightly higher. This result further confirms that the robust optimum differs from the deterministic one and that the statistical performance is indeed improved.

Fig. 7 provides an insightful visualisation of how the manoeuvres and observation arcs affect the flyby uncertainties. In particular, the figure shows, on the y-axis, the Semi-MAjor Axis (SMAA) and Semi-MInor Axis (SMIA) of the B-plane 1-σ confidence ellipse, and of the uncertainty on the hyperbolic TCA for different times along the trajectory (x-axis), if no other action is taken after that time. The observation instances are represented with vertical dashed black lines, while manoeuvres are indicated by black solid lines. The value of the mapped uncertainty is around 10 km and 500 m in SMAA and SMIA, and 10 seconds in TCA, as resulting purely from the initial dispersion as in Table 1. The

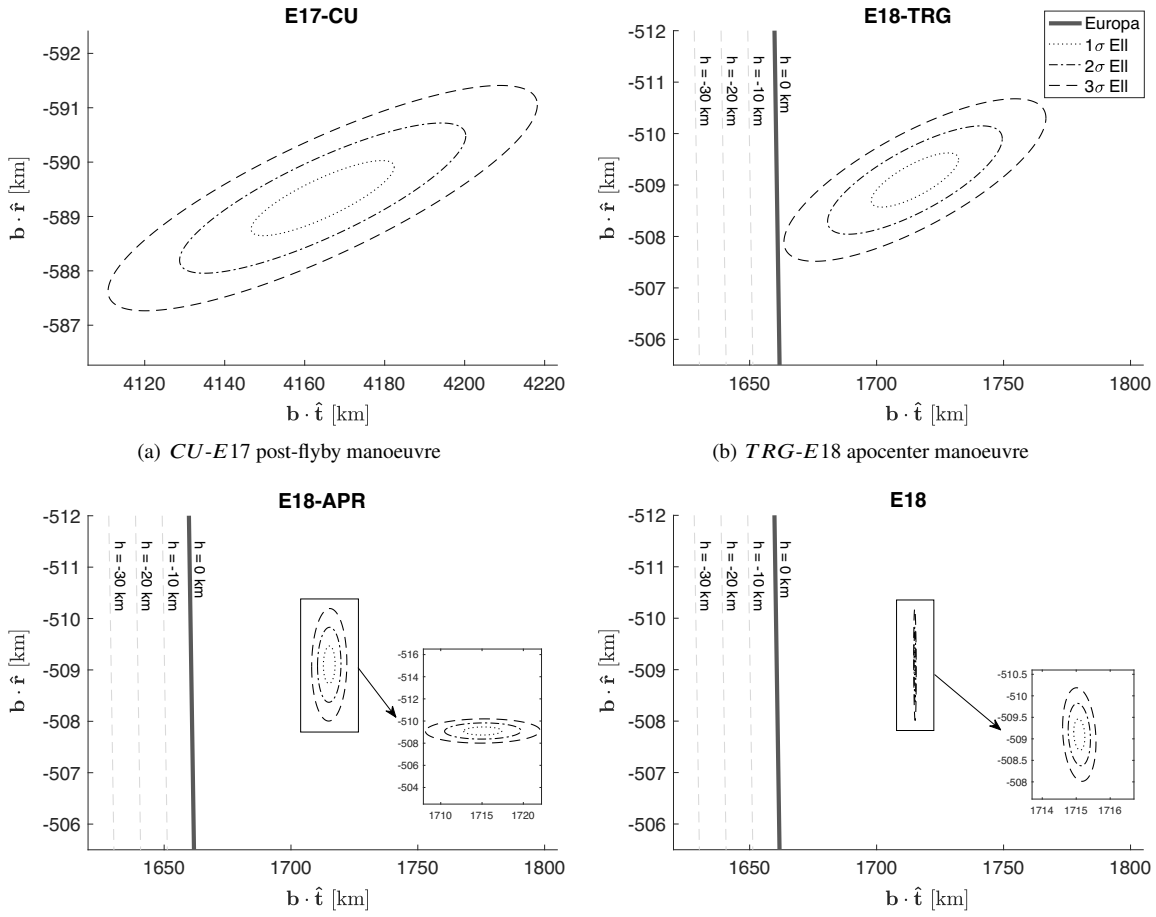

(a) CU-$E17$ post-flyby manoeuvre

(b) TRG-$E18$ apocenter manoeuvre

(c) APR-$E18$ approach manoeuvre

(d) $E18$ closest approach

Fig. 6 Confidence ellipses in B-vector components mapped from different instances of the robust trajectory without successive manoeuvres and observations under aleatory uncertainty.

Table 5 Free variables, open-loop magnitude $\Delta\overline{v}$, total $\Delta v99$, their ratio and PoI for verification solution without imposing the PoI constraint.

Solution	Aleatory Robust w/o PoI
$\Delta\overline{\mathbf{v}}_{CU\text{-}E17}$ [m/s]	[0.0 , −0.01, −0.01]
$\Delta\overline{\mathbf{v}}_{TRG\text{-}E18}$ [m/s]	[−1.28, +2.89, +3.25]
$\Delta\overline{\mathbf{v}}_{CU\text{-}E18}$ [m/s]	[−0.04, −0.02, +0.03]
$\Delta\overline{v}$ [m/s]	4.60
$\Delta v99$ [m/s]	8.02
$\Delta v99/\Delta\overline{v}$ [-]	1.74
PoI [-]	0.76%

mapped uncertainty exhibits then a jump at E17, the time of the clean-up manoeuvre, because of the executions errors. Successively, the orbit determination arcs reduce the B-plane ellipsoid by more than one order of magnitude in SMAA

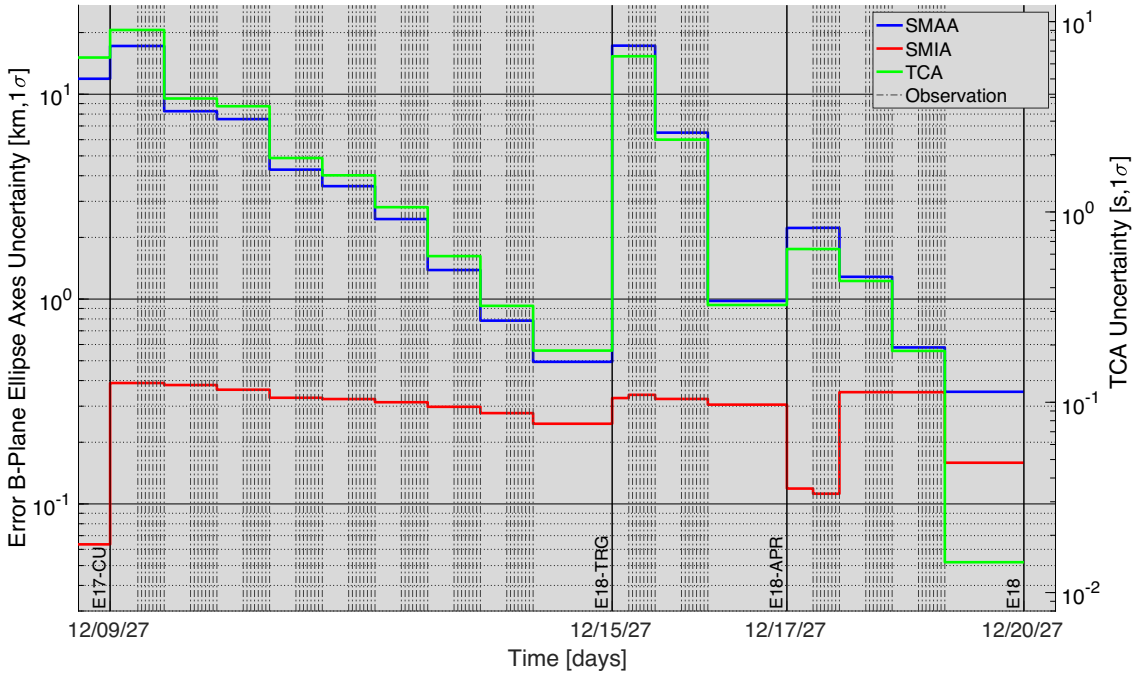

Fig. 7 Uncertainty mapped from different times during the robust trajectory to the reference flyby time and transformed in B-plane coordinates.

and TCA, whereas the reduction in SMIA is more contained. The main targeting manoeuvre $\Delta\bar{\mathbf{v}}_{TRG\text{-}E18}$ and its high execution errors cause a major spike in the delivered uncertainty. The values of SMAA and SMIA at this event are critical for the robust optimisation process, as this B-plane mapped uncertainty is the one employed for the probability of impact computation. Successive OD arcs help to reduce significantly the SMAA and TCA mapped dispersion until another, more contained, jump at the approach manoeuvre before E18. Finally, the measurements arcs before E18 reduce the mapped uncertainty even further, to have an expected 1-σ uncertainty at flyby of a few hundred meters in SMAA and SMIA, and a few tenths of a second for the TCA.

2. Mixed aleatory and epistemic uncertainty

Starting from the same deterministic solution we now introduce epistemic uncertainties in the distributions and solve the full problem (53). In this case, for the deterministic solution reported in Table 6 we have $\overline{\text{PoI}} = 2.29\% \not< 0.1\%$, which violates the impact constraint even more severely than in the aleatory case. The total ΔV_{tot} that provides the required percentile $\Delta v99$ is significantly higher than the one in the purely aleatory case, mainly due to the larger execution errors.

The corresponding B-plane uncertainty ellipses mapped and delivered from the manoeuvre instances along the trajectory are visualised in Fig. 8. For each subfigure, multiple 3-σ ellipsoids are represented by taking samples of the epistemic parameters within their intervals (see Table 2) and running a navigation analysis for each epistemic value. By

Table 6 Free variables, open-loop magnitude $\Delta\overline{v}$, total $\overline{\Delta v99}$, their ratio and upper PoI for first guess under epistemic uncertainty.

Solution	Epistemic First Guess
$\Delta\overline{\mathbf{v}}_{CU\text{-}E17}$ [m/s]	[0.0 , 0.0 , 0.0]
$\Delta\overline{\mathbf{v}}_{TRG\text{-}E18}$ [m/s]	$[-1.30, +2.86, +3.23]$
$\Delta\overline{\mathbf{v}}_{CU\text{-}E18}$ [m/s]	[0.0 , 0.0 , 0.0]
$\Delta\overline{v}$ [m/s]	4.51
$\overline{\Delta v99}$ [m/s]	8.65
$\overline{\Delta v99}/\Delta\overline{v}$ [-]	1.92
$\overline{\text{PoI}}$ [-]	2.29%

comparing Fig 5 with Fig. 8, one can see that in every subplot the ellipses change in size and, at times, rotate due to the epistemic uncertainty. For the chance constraint on the $\overline{\text{PoI}}$ after targeting, the inner optimisation routine looks for the epistemic sample which yields the ellipse with the largest intersection with the equivalent Europa surface in Fig. 8(b).

The main features of the BOC solution to problem (53) are reported in Table 7. Again, the values of the expected value constraints are not reported as they are met up to the required threshold, that is the new trajectory respects the required flyby conditions and final position in expected value. The average wall time for computing the BOC solution increases to 11 minutes under epistemic uncertainty.

Table 7 Free variables, open-loop magnitude $\Delta\overline{v}$, total $\overline{\Delta v99}$, their ratio and upper PoI for robust solution under epistemic uncertainty.

Solution	Epistemic Robust
$\Delta\overline{\mathbf{v}}_{CU\text{-}E17}$ [m/s]	$[-0.35, +1.12, +0.16]$
$\Delta\overline{\mathbf{v}}_{TRG\text{-}E18}$ [m/s]	$[-1.73, +1.57, +1.30]$
$\Delta\mathbf{v}_{CU\text{-}E18}$ [m/s]	$[+1.43, -2.13, -3.24]$
$\Delta\overline{v}$ [m/s]	7.99
$\overline{\Delta v99}$ [m/s]	14.76
$\overline{\Delta v99}/\Delta\overline{v}$ [-]	1.84
$\overline{\text{PoI}}$ [-]	0.04%

The $\overline{\text{PoI}}$ constraint is satisfied by trading part of the targeting manoeuvre with the E17 and E18 clean-up manoeuvres. The latter is now the largest manoeuvre employed to steer the spacecraft back to the desired final conditions. The value of $\Delta v99$ is significantly higher than in the aleatory case in Table 4 due to:

- the more severe uncertainty coming from the unknown probability distribution;
- the larger execution errors causing bigger deviations and, therefore, higher statistical manoeuvres.

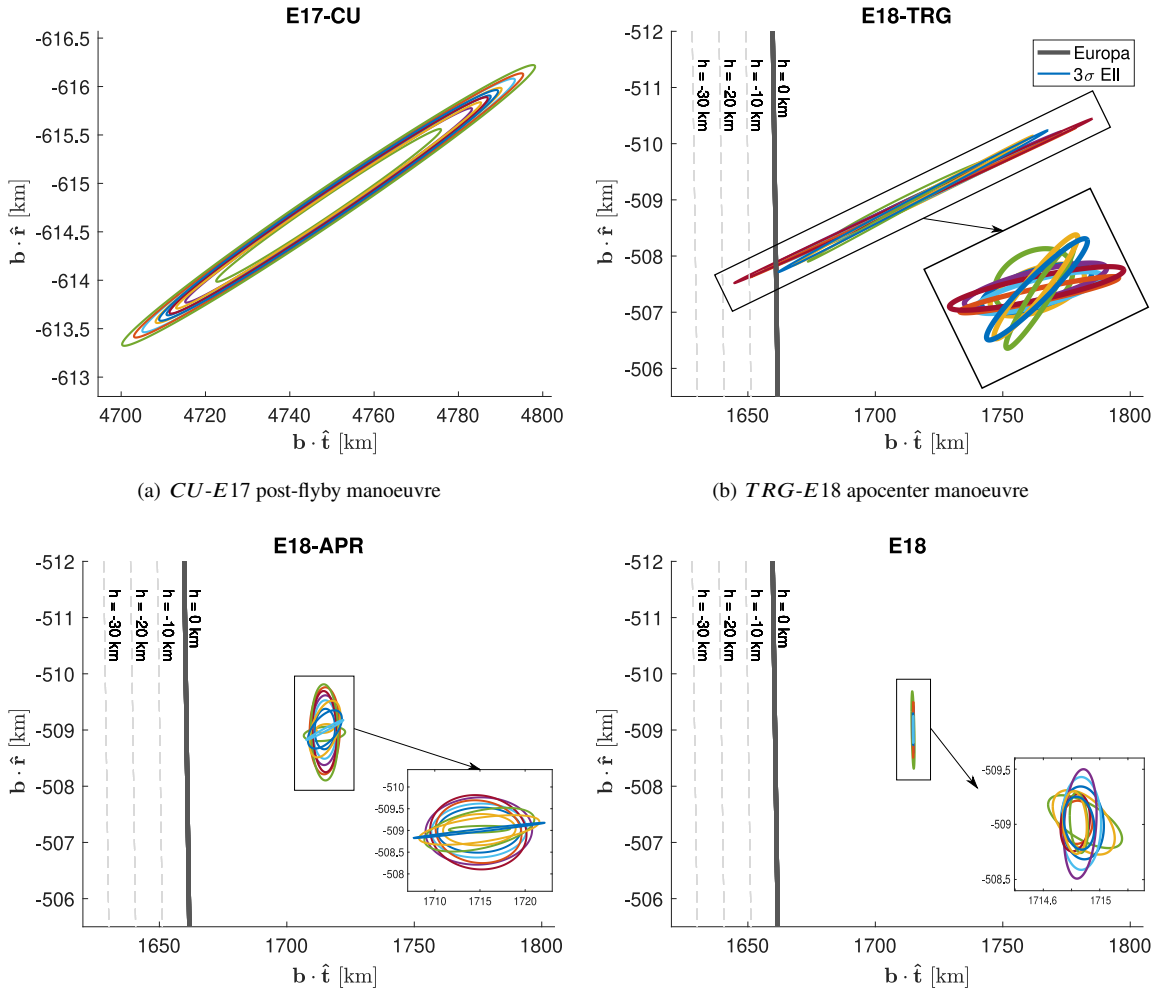

(a) CU-$E17$ post-flyby manoeuvre

(b) TRG-$E18$ apocenter manoeuvre

(c) APR-$E18$ approach manoeuvre

(d) $E18$ closest approach

Fig. 8 Confidence ellipses in B-vector components mapped from different instances of the first guess trajectory without successive manoeuvres and observations under epistemic uncertainty.

A visualisation of the 3-σ uncertainty ellipses on the B-plane for the robust solution can be found in Fig. 9, where again each ellipsoid results from a different value of the epistemic parameters. By comparing this plot with Fig. 8, Fig. 9(a) displays an evident change in the B-plane parameters after E17-CU, as the larger clean-up manoeuvre steers the delivered uncertainty closer to the target flyby conditions. Fig. 9(b), representing the mapped uncertainty after targeting, shows that there is no intersection between the largest 3-σ ellipse and the equivalent surface of Europa, confirming that the PoI constraint is met also in the epistemic case. Similarly to the precise case, the ellipses have smaller semi-major axes, larger semi-minor axes and are rotated counterclockwise to reduce the $\overline{\text{PoI}}$ while keeping the mean on the desired flyby conditions. Figure 9(c) reveals an increase in the delivered uncertainty after approach due to the larger statistical manoeuvres. Finally, Fig. 9(d) shows how the range and range-rate observations reduce the reconstructed uncertainty at flyby, mainly in the $\mathbf{b} \cdot \hat{\mathbf{t}}$ component.

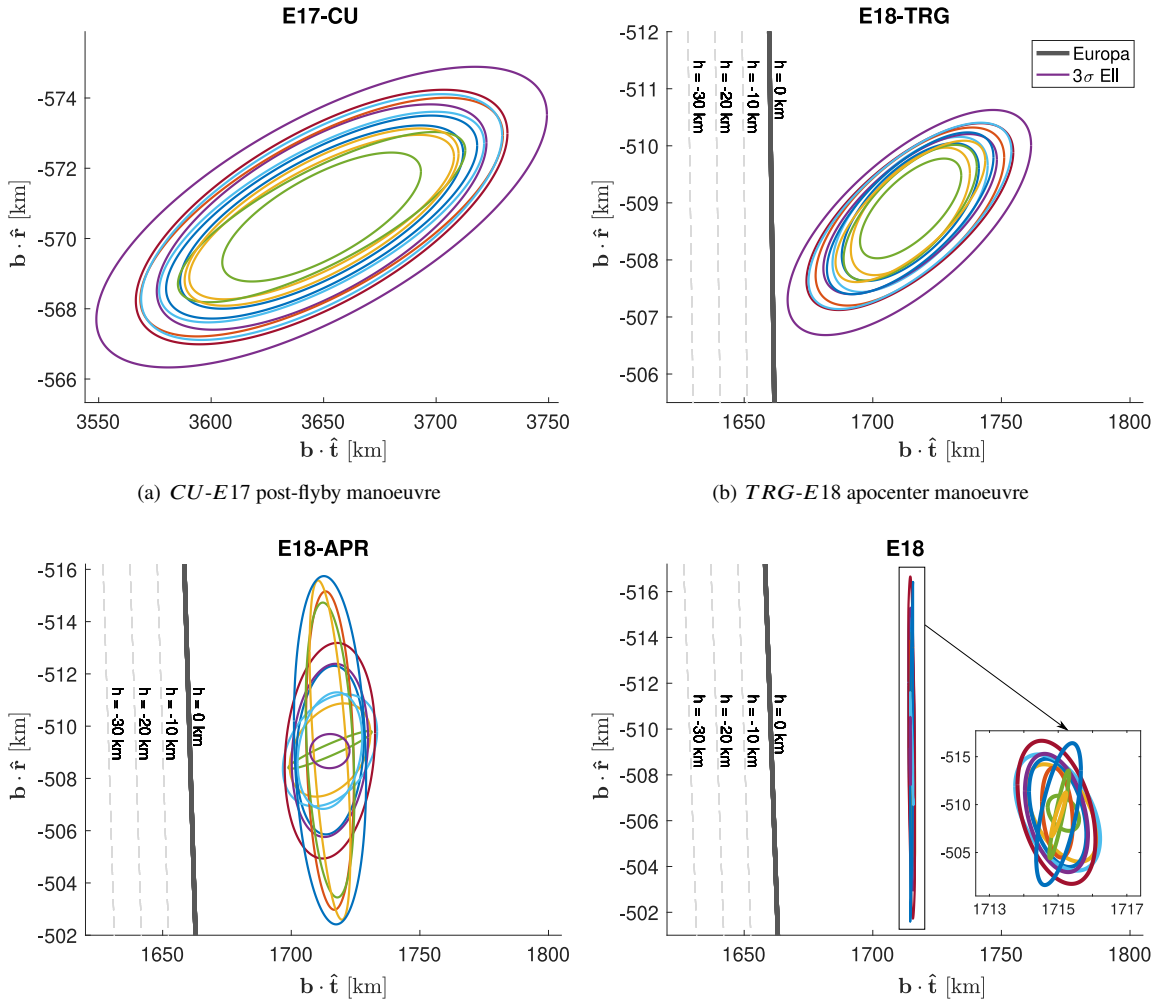

(a) CU-$E17$ post-flyby manoeuvre

(b) TRG-$E18$ apocenter manoeuvre

(c) APR-$E18$ approach manoeuvre

(d) $E18$ closest approach

Fig. 9 Confidence ellipses in B-vector components mapped from different instances of the robust trajectory without successive manoeuvres and observations under epistemic uncertainty.

V. Conclusions

This paper proposed a novel development in optimal control problems under uncertainty for the design of space trajectories. The main contribution of this work is the development of the BOC formulation and the generalisation of a shooting-like stochastic transcription to the case of orbit determination arcs and statistical controllers.

It was shown that the proposed belief-based formulation can accommodate both aleatory and epistemic and allows the treatment of families of probability measures since no assumptions are made on the nature of the probability distributions describing the uncertainties, or on the transition function to propagate them. This formulation further enables the optimisation of the *open-loop* thrust profile taking into account the effect of *closed-loop* components in continuous state space applications with sparse observations, thus coupling the trajectory optimisation process with the navigation analysis. Indeed, a belief-based model is particularly suited to model the inference step necessary for the

state knowledge update when an orbit determination campaign is carried out.

The proposed transcription was generalised to the presence of orbit determination by adapting the shooting-like discretisation through propagation and inference maps. A sparse polynomial mapping was employed to propagate the belief state through the nonlinear dynamics. The developed scheme was shown to transcribe the continuous problem under uncertainty in a discrete form to be optimised with a local NLP solver.

The optimised solution resulting from this approach is highly informative as it determines the nominal control profile given a predefined control policy for possible deviations due to uncertainty, hence directly providing multiple control laws and the associated empirical margins for correction manoeuvres.

On the re-design of the Europa Clipper flyby tour, the BOC formulation was shown to simultaneously optimise the total cost of the executed manoeuvres and to satisfy all constraints under both aleatory and epistemic uncertainty. The BOC was able to solve for the initial infeasibility in PoI of the deterministic solution, and find a robust trajectory that simultaneously satisfies the statistical constraints and minimises the $\Delta v99$, that is the .99 quantile for the total cost of the manoeuvres. As a verification, it was shown that the BOC solution outperforms the deterministic initial guess when no PoI constraint is considered.

The optimisation over the epistemic set is currently carried out using a local search, although this problem is often multimodal. Therefore, future developments will include a global solver for the outer optimisation loop to find the lower and upper bounds of the quantity of interest. Furthermore, additional work will revolve around the development of an efficient epistemic estimator for Bayesian inference to replace the current Monte Carlo sampling over the observation and include epistemic uncertainty in the measurements more efficiently. Both theoretical and empirical complexity analyses should be carried out to formally assess the scalability of the method with the number of aleatory, epistemic, and control parameters. Future theoretical work will also focus on the development of belief optimal control for continuous thrust problems, which are characterised by more challenging operational constraints and increased dimensionality of the transcribed optimisation. Finally, additional uncertainty sources will be considered for future applications, e.g., errors in the time of execution of the manoeuvres and in the ephemerides of the moons.

A. B-plane coordinate tranformation

The B-plane is the plane passing through the target body center of mass and perpendicular to the hyperbola incoming asymptote [55, 62, 63]. It is defined by three unit vectors: $\hat{\mathbf{s}}$ is the unit vector parallel to the relative incoming asymptote with positive direction aligned to the incoming asymptotic velocity; $\hat{\mathbf{t}}$ is the cross product between $\hat{\mathbf{s}}$ and the normal to the ecliptic, that is $\hat{\mathbf{z}}$ vector in the inertial frame; $\hat{\mathbf{r}}$ is the cross product between $\hat{\mathbf{s}}$ and $\hat{\mathbf{t}}$.

The transformation from inertial to B-plane coordinates is

$$\mathbf{B} = [\,\mathbf{b},\, \mathrm{TCA}] = \mathcal{B}(\mathbf{x}(t))\ ,$$

where the *aiming point* $\mathbf{b} = (\mathbf{b} \cdot \hat{\mathbf{t}})\,\hat{\mathbf{t}} + (\mathbf{b} \cdot \hat{\mathbf{r}})\,\hat{\mathbf{r}}$ is the target-centered vector to the intersection point between the incoming asymptote and the B-plane (it would be the closest approach point if the target body were massless), whereas the hyperbolic TCA is the time interval that the spacecraft needs to travel from $\mathbf{x}(t)$ to the flyby closest approach along the relative hyperbolic orbit.

The transformation $\mathcal{B}$ therefore returns the two components, $\mathbf{b} \cdot \hat{\mathbf{t}}$ and $\mathbf{b} \cdot \hat{\mathbf{r}}$, and the hyperbolic TCA for a given inertial state $\mathbf{x}$ in the proximity of the flyby. First the inertial state with respect to the central body is converted to the inertial state with respect to the target body to flyby by a simple translation. Hence, let $\mathbf{r}$ and $\mathbf{v}$ be the relative position and velocity of the spacecraft. Then, following [62], the unit vectors are first derived by computing the unit normal vector

$$\hat{\mathbf{h}} = \mathbf{r} \times \mathbf{v} \,/\, \|\mathbf{r} \times \mathbf{v}\| \,,$$

the eccentricity vector

$$\mathbf{e} = \left(\frac{v^2}{\mu} - \frac{1}{r}\right)\mathbf{r} - \frac{(\mathbf{r} \cdot \mathbf{v})}{\mu}\mathbf{v} \,,$$

and the asymptote angle

$$\beta = \cos^{-1}(1/e) \,.$$

Hence, $\hat{\mathbf{s}}$ can be written as

$$\hat{\mathbf{s}} = \cos\beta \frac{\mathbf{e}}{\|\mathbf{e}\|} + \sin\beta \frac{\hat{\mathbf{h}} \times \mathbf{e}}{\|\hat{\mathbf{h}} \times \mathbf{e}\|} \,,$$

and consequently

$$\hat{\mathbf{t}} = \hat{\mathbf{s}} \times \hat{\mathbf{z}}$$

$$\hat{\mathbf{r}} = \hat{\mathbf{s}} \times \hat{\mathbf{t}} \,.$$

Hence, from the hyperbolic semi-major axis

$$a = -\frac{\mu}{2} \Big/ \left(\frac{v^2}{2} - \frac{\mu}{2}\right) \,,$$

the $\mathbf{b}$ vector magnitude is computed as

$$\|\mathbf{b}\| = \frac{\|\mathbf{h}\|}{v_\infty} = -a\sqrt{e^2 - 1} \,.$$

Begin the aiming point within the B-plane (perpendicular to $\hat{\mathbf{s}}$) and within the relative orbital motion (perpendicular to $\hat{\mathbf{h}}$), the $\mathbf{b}$ vector can be finally written as

$$\mathbf{b} = \|\mathbf{b}\| \left(\hat{\mathbf{s}} \times \hat{\mathbf{h}}\right) \,,$$

and its projections onto $\hat{\mathbf{t}}$ and $\hat{\mathbf{r}}$ can be found by a scalar product. The hyperbolic TCA is computed by the relation

between hyperbolic anomaly H and time (see Equation (8.23-1) of [63])

$$\mathrm{TCA} = \frac{e \sinh H - H}{\sqrt{\mu/a^3}} ,$$

where H is derived by its definition

$$r = a(1 - e \cosh H) .$$

As the B-plane change of coordinates involves only algebric passages, the Jacobian of this transformation with respect to the inertial state

$$J_{\mathcal{B}} = \frac{\partial \mathbf{B}}{\partial \mathbf{x}}$$

can computed analytically. Specifically, the derivative of the equations above with respect to the parameters appearing on the right-hand side are derived by symbolic differentiation, and the Jacobian is constructed by chain rule.

Funding Sources

Stefano Campagnola acknowledges the support from JPL's Research and Technology Development funds and from the Clipper project; part of this research was carried out at the Jet Propulsion Laboratory, California Institute of Technology, under a contract with the National Aeronautics and Space Administration. This work was partially funded by the European Commission's H2020 programme, through the H2020-MSCA-ITN-2016 UTOPIAE Marie Curie Innovative Training Network, grant agreement 722734.

Acknowledgements

The authors would like to thank Eric Gustafson, Sonia Hernandez, Frank Laipert, Sumita Nandi, and Brian Young for sharing their expertise in navigation analysis and modelling for the addressed application, and for the insightful discussions during the approach development.

References

[1] Rayman, M. D., and Williams, S. N., "Design of the first interplanetary solar electric propulsion mission," *Journal of Spacecraft and Rockets*, Vol. 3, 2002, pp. 589–595. https://doi.org/10.2514/2.3848.

[2] Laipert, F. E., and Longuski, J. M., "Automated Missed-Thrust Propellant Margin Analysis for Low-Thrust Trajectories," *Journal of Spacecraft and Rockets*, Vol. 52, 2015, pp. 1135–1143. https://doi.org/10.2514/1.A33264.

[3] Campagnola, S., Ozaki, N., Sugimoto, Y., Yam, C. H., Chen, H., Kawabata, Y., Ogura, S., Sarli, B., Kawakatsu, Y., Funase, R., and Nakasuka, S., "Low-thrust trajectory design and operations of PROCYON, the first deep-space micro-spacecraft," *24th International Symposium on Space Flight Dynamics*, Munich, Germany, 2015.

[4] Campagnola, S., Hernando-Ayuso, J., Kakihara, K., Kawabata, Y., Chikazawa, T., Funase, R., Ozaki, N., Baresi, N., Hashimoto, T., Kawakatsu, Y., Ikenaga, T., Oguri, K., and Oshima, K., "Mission analysis for the EM-1 CubeSats EQUULEUS and OMOTENASHI," *IEEE Aerospace and Electronic Systems Magazine*, Vol. 34, No. 4, 2019. https://doi.org/10.1109/MAES.2019.2916291.

[5] Guo, J., Monas, L., and Gill, E., "Statistical analysis and modelling of small satellite reliability," *Acta Astronautica*, Vol. 98, 2014, pp. 97–110. https://doi.org/10.1016/j.actaastro.2014.01.018.

[6] Richards, A., and How, J., "Robust stable model predictive control with constraint tightening," *American Control Conference 2006 IEEE*, 2006. https://doi.org/10.1109/ACC.2006.1656440.

[7] Gustafson, E. D., "Stochastic Optimal Control of Spacecraft," Ph.D. thesis, The University of Michigan, 2010. https://doi.org/2027.42/77707.

[8] Ozaki, N., Campagnola, S., Funase, R., and Yam, C. H., "Stochastic Differential Dynamic Programming with Unscented Transform for Low-Thrust Trajectory Design," *Journal of Guidance, Control, and Dynamics*, Vol. 41, 2018, pp. 377–387. https://doi.org/10.2514/1.G002367.

[9] Ozaki, N., Campagnola, S., and Funase, R., "Tube Stochastic Optimal Control for Nonlinear Constrained Trajectory Optimization Problems," *Journal of Guidance, Control, and Dynamics*, Vol. 43, No. 4, 2020, pp. 645–655. https://doi.org/10.2514/1.G004363.

[10] Okamoto, K., Goldshtein, M., and Tsiotras, P., "Optimal Covariance Control for Stochastic Systems Under Chance Constraints," *IEEE Control Systems Letters*, Vol. 2, No. 2, 2018, pp. 266–271. https://doi.org/10.1109/LCSYS.2018.2826038.

[11] Yi, Z., Cao, Z., Theodorou, E., and Chen, Y., "Nonlinear Covariance Control via Differential Dynamic Programming," *2020 American Control Conference (ACC)*, 2020. https://doi.org/10.23919/ACC45564.2020.9147531.

[12] Jenson, E. L., Chen, X., and Scheeres, D. J., "Optimal Spacecraft Guidance With Asynchronous Measurements and Noisy Impulsive Controls," *IEEE Control Systems Letters*, Vol. 5, No. 5, 2021, pp. 1813–1818. https://doi.org/10.1109/LCSYS.2020.3045384.

[13] Jenson, E. L., and Scheeres, D. J., "Multi-Objective Optimization of Covariance and Energy for Asteroid Transfers," *Journal of Guidance, Control, and Dynamics*, Vol. 44, No. 7, 2021, pp. 1253–1265. https://doi.org/10.2514/1.G005609.

[14] Oguri, K., and McMahon, J. W., "Robust Spacecraft Guidance Around Small Bodies Under Uncertainty: Stochastic Optimal Control Approach," *Journal of Guidance, Control, and Dynamics*, Vol. 44, No. 7, 2021, pp. 1295–1313. https://doi.org/10.2514/1.G005426.

[15] Oguri, K., and McMahon, J. W., "Risk-aware Trajectory Design with Continuous Thrust: Primer Vector Theory Approach," *AAS/AIAA Astrodynamics Specialist Conference*, 2019.

[16] Olympio, J. T., and Yam, C. H., "Deterministic method for space trajectory design with mission margin constraints," *61st International Astronautical Congress*, Prague, Czech Republic, 2010.

[17] Olympio, J. T., "Designing Robust Low-Thrust Interplanetary Trajectories Subject to One Temporary Engine Failure," *20th AAS/AIAA Space Flight Meeting*, San Diego, CA, US, 2010.

[18] Di Lizia, P., Armellin, R., Bernelli-Zazzera, F., and Berz, M., "High order optimal control of space trajectories with uncertain boundary conditions," *Acta Astronautica*, Vol. 93, 2014, pp. 217–229. https://doi.org/10.1016/j.actaastro.2013.07.007.

[19] Rubinsztejn, A., Sandel, C. G., Sood, R., and Laipert, F. E., "Designing trajectories resilient to missed thrust events using expected thrust fraction," *Aerospace Science and Technology*, Vol. 115, 2021, p. 106780. https://doi.org/10.1016/j.ast.2021.106780.

[20] Rubinsztejn, A., Sood, R., and Laipert, F. E., "Expected thrust fraction: resilient trajectory design applied to the Earth return orbiter," *31st AAS/AIAA Space Flight Mechanics Meeting*, 2021.

[21] Izzo, D., Märtens, M., and Pan, B., "A survey on artificial intelligence trends in spacecraft guidance dynamics and control," *Astrodynamics*, Vol. 3, No. 4, 2019, pp. 287–299. https://doi.org/10.1007/s42064-018-0053-6.

[22] Rubinsztejn, A., Sood, R., and Laipert, F. E., "Neural network optimal control in astrodynamics: Application to the missed thrust problem," *Acta Astronautica*, Vol. 176, 2020, pp. 192–203. https://doi.org/10.1016/j.actaastro.2020.05.027.

[23] Izzo, D., and Öztürk, E., "Real-Time Guidance for Low-Thrust Transfers Using Deep Neural Networks," *Journal of Guidance, Control, and Dynamics*, Vol. 44, No. 2, 2021, pp. 315–327. https://doi.org/10.2514/1.G005254.

[24] Miller, D., and Linares, R., "Low-thrust optimal control via reinforcement learning," *29th AAS/AIAA Space Flight Mechanics Meeting*, American Astronautical Society Ka'anapali, Hawaii, 2019.

[25] Zavoli, A., and Federici, L., "Reinforcement Learning for Robust Trajectory Design of Interplanetary Missions," *Journal of Guidance, Control, and Dynamics*, Vol. 44, No. 8, 2021, pp. 1440–1453. https://doi.org/10.2514/1.G005794.

[26] Vasile, M., "Robustness optimisation of aerocapture trajectory design using a hybrid co-evolutionary approach," *18th International Symposium on Space Flight Dynamics*, Munich, Germany, 2004.

[27] Zuiani, F., Vasile, M., and Gibbings, A., "Evidence-based robust design of deflection actions for near Earth objects," *Celestial Mechanics and Dynamical Astronomy*, Vol. 114, 2012, pp. 107–136. https://doi.org/10.1007/s10569-012-9423-1.

[28] Di Carlo, M., Vasile, M., Greco, C., and Epenoy, R., "Robust optimisation of low-thrust interplanetary transfers using evidence theory," *29th AAS/AIAA Space Flight Mechanics Meeting*, Ka'anapali, Hawaii, US, 2019. URL strathprints:67543.

[29] Graça Marto, S., Vasile, M., and Epenoy, R., "Multi-objective robust trajectory optimisation under epistemic uncertainty and imprecision," *Proceedings of the 70th International Astronautical Congress, IAC19*, Washington, DC, US, 2019. URL strathprints:70454.

[30] Kaelbling, L. P., Littman, M. L., and Cassandra, A. R., "Planning and acting in partially observable stochastic domains," *Artificial intelligence*, Vol. 101, No. 1-2, 1998, pp. 99–134. https://doi.org/10.1016/S0004-3702(98)00023-X.

[31] Greco, C., Di Carlo, M., Vasile, M., and Epenoy, R., "An intrusive polynomial algebra multiple shooting approach to the solution of optimal control problems," *Proceedings of the 69th International Astronautical Congress, IAC18*, Bremen, Germany, 2018. URL strathprints:65918.

[32] Greco, C., Di Carlo, M., Vasile, M., and Epenoy, R., "Direct multiple shooting transcription with polynomial algebra for optimal control problems under uncertainty," *Acta Astronautica*, Vol. 170, 2020, pp. 224–234. https://doi.org/10.1016/j.actaastro.2019.12.010.

[33] Gelb, A., *Applied optimal estimation*, MIT press, 1974. Chap. 7.

[34] Stastny, N. B., and Geller, D. K., "Autonomous Optical Navigation at Jupiter: A Linear Covariance Analysis," *Journal of Spacecraft and Rockets*, Vol. 45, No. 2, 2008, pp. 290–298. https://doi.org/10.2514/1.28451.

[35] Geller, D. K., "Linear Covariance Techniques for Orbital Rendezvous Analysis and Autonomous Onboard Mission Planning," *Journal of Guidance, Control, and Dynamics*, Vol. 29, No. 6, 2006, pp. 1404–1414. https://doi.org/10.2514/1.19447.

[36] Campagnola, S., Buffington, B. B., Lam, T., Petropoulos, A. E., and Pellegrini, E., "Tour Design Techniques for the Europa Clipper Mission," *Journal of Guidance, Control, and Dynamics*, 2019, pp. 1–12. https://doi.org/10.2514/1.G004309.

[37] Bagchi, A., *Optimal control of stochastic systems*, Prentice Hall International (UK) Limited, 1993.

[38] Frank, T. D., *Nonlinear Fokker-Planck equations: fundamentals and applications*, Springer Science & Business Media, 2005.

[39] Krishnamurthy, V., *Partially observed Markov decision processes*, Cambridge University Press, 2016.

[40] Tapley, B., Schutz, B., and Born, G. H., *Statistical orbit determination*, Elsevier, 2004.

[41] Greco, C., Gentile, L., Filippi, G., Minisci, E., Vasile, M., and Bartz-Beielstein, T., "Autonomous generation of observation schedules for tracking satellites with structured-chromosome GA optimisation," *2019 IEEE Congress on Evolutionary Computation (CEC)*, 2019. https://doi.org/10.1109/CEC.2019.8790101.

[42] Vasile, M., Ortega Absil, C., and Riccardi, A., "Set propagation in dynamical systems with generalised polynomial algebra and its computational complexity," *Communications in Nonlinear Science and Numerical Simulation*, Vol. 75, 2019, pp. 22–49. https://doi.org/10.1016/j.cnsns.2019.03.019.

[43] Bäck, J., Nobile, F., Tamellini, L., and Tempone, R., "Stochastic spectral Galerkin and collocation methods for PDEs with random coefficients: a numerical comparison," *Spectral and High Order Methods for Partial Differential Equations*, Lecture Notes in Computational Science and Engineering, Vol. 76, edited by J. Hesthaven and E. Ronquist, Springer, 2011, pp. 43–62.

[44] Smolyak, S. A., "Quadrature and interpolation formulas for tensor products of certain classes of functions," *Soviet Mathematics Doklady*, Vol. 4, 1963.

[45] Bäck, J., Nobile, F., Tamellini, L., and Tempone, R., "Sparse Grids Matlab Kit," , 2021. https://sites.google.com/view/sparse-grids-kit.

[46] Ortega, C. A., Serra, R., Riccardi, A., and Vasile, M., "De-orbiting and re-entry analysis with generalised intrusive polynomial expansions," *67th International Astronautical Congress*, 2016. URL strathprints:60596.

[47] Riccardi, A., Tardioli, C., and Vasile, M., "An intrusive approach to uncertainty propagation in orbital mechanics based on Tchebycheff polynomial algebra," *Advances in Astronautical Sciences*, 2015, pp. 707–722. URL strathprints:60560.

[48] Valerino, P. N., Buffington, B., Criddle, K., Hahn, Y., Ionasescu, R., Kangas, J. A., Martin-Mur, T., Roncoli, R. B., and Sims, J. A., "Preliminary Maneuver Analysis for the Europa Clipper Multiple-Flyby Mission," *AIAA/AAS Astrodynamics Specialist Conference*, 2014. https://doi.org/10.2514/6.2014-4461.

[49] Nandi, S., Kangas, J., Valerino, P. N., Buffington, B., Ionasescu, R., and Boone, D., "Initial navigation analysis for the Europa multiple flyby mission concept," *26th AAS/AIAA Space Flight Mechanics Meeting*, 2016.

[50] Jeffrey, R. C., *The Logic of Decision*, 2nd ed., University of Chicago Press, 1983.

[51] Sarkka, S., *Bayesian Filtering and Smoothing*, 1st ed., Cambridge University Press, New York, 2013.

[52] Ito, K., and Xiong, K., "Gaussian filters for nonlinear filtering problems," *IEEE Transactions on Automatic Control*, Vol. 45, No. 5, 2000, pp. 910–927. https://doi.org/10.1109/9.855552.

[53] Julier, S. J., Uhlmann, J. K., and Durrant-Whyte, H. F., "A new approach for filtering nonlinear systems," *Proceedings of 1995 American Control Conference-ACC'95*, Vol. 3, IEEE, 1995.

[54] Lam, T., Buffington, B., and Campagnola, S., "A robust mission Tour for NASA's planned Europa Clipper mission," *2018 Space Flight Mechanics Meeting*, 2018.

[55] Lynam, A. E., and Longuski, J. M., "Preliminary analysis for the navigation of multiple-satellite-aided capture sequences at Jupiter," *Acta Astronautica*, Vol. 79, 2012, pp. 33–43. https://doi.org/10.1016/j.actaastro.2012.04.012.

[56] Acton, C., Bachman, N., Semenov, B., and Wright, E., "A look towards the future in the handling of space science mission geometry," *Planetary and Space Science*, Vol. 150, 2018, pp. 9–12.

[57] Gates, C. R., "A simplified model of midcourse maneuver execution errors," Tech. rep., Jet Propulsion Laboratory, California Institute of Technology, 1963.

[58] Goodson, T. D., "Execution-error modeling and analysis of the GRAIL spacecraft pair," *23rd AAS/AIAA Spaceflight Mechanics Meeting, Kauai, Hawaii*, 2013.

[59] Boone, D. R., Nandi, S., Kangas, J., and Young, B., "Orbit Determination Sensitivity Analysis for the Europa Multiple Flyby Mission Concept," *AIAA/AAS Astrodynamics Specialist Conference*, 2016. https://doi.org/10.2514/6.2016-5429.

[60] Wagner, S. V., "Cassini Maneuver performance assessment and execution-error modeling through 2015," *26th AAS/AIAA Space Flight Mechanics Meeting*, Napa, CA, US, 2016.

[61] Farnocchia, D., Eggl, S., Chodas, P. W., Giorgini, J. D., and Chesley, S. R., "Planetary encounter analysis on the B-plane: a comprehensive formulation," *Celestial Mechanics and Dynamical Astronomy*, Vol. 131, No. 8, 2019, p. 36.

[62] Cho, D.-H., Chung, Y., and Bang, H., "Trajectory correction maneuver design using an improved B-plane targeting method," *Acta Astronautica*, Vol. 72, 2012, pp. 47–61.

[63] Wakker, K. F., *Fundamentals of astrodynamics*, TU Delft Library, 2015.